AD NUMBER
AD007797
CLASSIFICATION CHANGES
TO: unclassified
FROM: confidential
LIMITATION CHANGES
TO: Approved for public release, distribution unlimited
FROM: Distribution authorized to DoD only; Administrative/Operational Use; 05 AUG 1952. Other requests shall be referred to Naval Ordnance Lab, White Oak, MD.
AUTHORITY
31 Aug 1964, DoDD 5200.10; 29 Aug 1974, st-a USNOL ltr

AD- 7797

CONFIDENTIAL

NAVORD REPORT 2305

ANALYSIS OF THE DRAG COMPONENTS OF THE ANGLED ARROW PROJECTILE

5 August 1952

U. S. NAVAL ORDNANCE LABORATORY
WHITE OAK, MARYLAND

CONFIDENTIAL

SECURITY INFORMATION

Aeroballistic Research Report 63

ANALYSIS OF THE DRAG COMPONENTS OF THE ANGLED ARROW PROJECTILE

Prepared by:

V. Halbmillion

ABSTRACT: This Report presents an analytical study of the drag components of the Angled Arrow Projectile under wind-tunnel testing conditions. Numerical results have been obtained for a range of Mach numbers between 1.5 and 4.5, and comparisons made with experimental data.

The estimated results are in good agreement with experimental data, but similar studies on other missiles will have to be made before it can be ascertained that the method of analysis is fully reliable. Of the drag components for the bare body, the contribution of the base pressure seems to be subject to the greatest uncertainty. In the case of wind-tunnel tests, the importance of the wave drag increases rapidly with the Mach number and contributes close to one-half of the total drag coefficient at $M = 4.5$. The behaviour of the base pressure drag is complicated by a strong Reynolds number effect, but its contribution drops rapidly at high Mach numbers. As the Mach number increases, the nature of the boundary layer around the missile changes from turbulent to laminar, with a corresponding drop of the skin friction coefficient, but once the boundary layer has stabilized, the contribution of the skin friction increases with the Mach number.

In the case of the finned body, the base pressure drag is again a very important factor, presently intractable analytically, and for which very few experimental data are available. The increase in drag due to the presence of the fins is considerable, varying from 50 to 70 percent of the bare body drag within the Mach number range considered (1.86 to 4.50).

U. S. NAVAL ORDNANCE LABORATORY
WHITE OAK, MARYLAND

NAVORD Report 2305 5 August 1952

The present Report is the first step in an attempt to predict analytically the drag characteristics of a finned missile. It considers the missile drag components at zero angle of attack of the missile relative to the air stream and zero angle of incidence of the fins relative to the body.

The method presented in this Report is used to estimate the drag of the Angled Arrow Projectile under wind-tunnel testing conditions.

This Report is for information only. It should be considered as of a preliminary nature, and the method presented will probably be modified and improved as the work proceeds.

The work presented in this Report falls under the task number NOL-Re3f-614-1-52.

EDWARD L. WOODYARD
Captain, USN
Commander

H. H. KURZWEG, Chief
Aeroballistic Research Department

CONTENTS

ILLUSTRATIONS

TABLES

Aeroballistic Research Report 63

ANALYSIS OF THE DRAG COMPONENTS OF THE ANGLED ARROW PROJECTILE

INTRODUCTION

1. The general purpose of the task, of which this Report presents the first part, is to determine the various components of the drag of a finned missile under both wind-tunnel and free-flight conditions. The final goal is to establish an analytical method of predicting the total drag under any flight or test conditions, and the influence of the Reynolds number on the final result. It is hoped in this way to get the answers to problems such as the following:

a. Given a certain finned missile, to determine the relative contributions of the wave drag, the skin friction, the base pressure, the fins, and how the ratios are affected by a change of scale.

b. Knowing the drag experimentally from, say, wind-tunnel tests, to predict the drag on the full-scale missile.

c. To permit the rapid estimation of a change in drag due to a minor change in the missile configuration, like a change in the leading edge sweep angle of the fins.

d. To draw conclusions on the possible means of reducing the drag of a given missile.

e. To establish a basis of comparison between the drags of different missiles.

2. The total drag coefficient of a finned missile is composed of the drag coefficient of the body alone (assuming the fins nonexistent) and the drag coefficient due to the presence of the fins. The latter drag is a complex combination involving:

a. The wave drag.

b. The skin friction.

c. The drag due to the normal force, also called lift drag.

d. The effect of the fins on the body drag (and especially the base pressure drag).

e. The effect of the body on the drag of the fins.

f. The cross-flow over body and fins, existing only when the missile flies with a certain angle of attack.

Part I

Drag Components for the Body Alone

3. The present report limits itself to the calculation of the drag components at zero angle of attack. These components for the body alone are as follows:

a. The wave or pressure drag, resulting from the pressure distribution created along the body.

b. The skin friction drag, due to the viscous forces in the boundary layer.

c. The base drag, resulting from the partial vacuum created in the wake behind the body.

These various components will be examined in detail and estimated separately.

4. The original body shape of the Angled Arrow Projectile (AAP), as tested in the NOL wind-tunnels, is composed of a tangent ogival nose of 16.25 calibers followed by a cylindrical afterbody. In the geometry of missiles, the diameter of the body is often taken as a unit of length and called a caliber. A "caliber number" of 16.25 indicates, therefore, that the radius of the arc of the circle generating the ogival nose is equal to 16.25 times the missile diameter. There is no boat-tail at the end of the cylindrical portion, so that the base area is equal to the maximum cross-sectional area of the bare body. The length of the cylindrical portion is six calibers. It can be shown from simple geometric considerations (reference (a)) that if N_c is the caliber number of an ogive, its axial length is given by $\sqrt{N_c - 1/4}$ Therefore, the length of the ogival nose is four calibers, and the total length of the missile is ten calibers.

The Body Wave Drag

5. Of all the drag components, the wave drag is the one which is the most susceptible of a rigorous analytical treatment. In order to compute the wave drag, it is necessary to know the pressure distribution over all the surfaces whose normal is not perpendicular to the direction of motion. This results from the definition of the drag itself. In the case of a non-yawing missile, which we are considering here, only the pressure distribution on the ogival portion of the missile is required, up to the point of tangency.

6. There is no simple analytical way to determine the pressure distribution around a given ogive at a given Mach number. But just as in the case of other pointed bodies of revolution, the pressure distribution can be determined with practically any degree of accuracy required by using the method of characteristics. The main drawback of the method is the very considerable amount of work involved, which makes it necessary at present to resort to one of the three approximate methods listed below.

Approximate Methods for the Determination of Pressure Distributions on Ogives

7. One method of obtaining a fairly rapid approximation of the value of the drag of an ogive is given by E. R. C. Miles in reference (b). Miles assumes that the pressure at the tip of the ogival nose is equal to that on a cone of the same nose angle, and therefore calculable by the classical theory of Taylor-Maccoll. He also assumes that, along the ogive, the $\Delta p/q_1$ varies linearly with the axial distance x. In other words, $\Delta p/q_1$ is of the form $ax+b$, where a is obtained empirically from experimental data, and b is the value of the wave drag coefficient for a cone of the same angle as the ogival angle at the nose tip, as computed by the method of Taylor-Maccoll. The formula for the wave drag offered by Miles is then

$$C_{D_W} = b\left[1 - \frac{2(49\lambda^2 - 16)}{7(M+18)\lambda^2}\right].$$

In this formula, M is the free-stream Mach number, and λ is the "slenderness" ratio, which is implicitly defined by Miles as the ratio of the axial length of the ogive to the radius of the body at the point of tangency between ogive and cylinder. λ is then equal to twice the axial length of the ogive expressed in calibers. The factor b can be obtained from the original curves of Taylor-Maccoll (reference (c)). These curves give b as a function of the Mach number, with the semi-nose-angle of the cone as the parameter. They have been reproduced in reference (b). Miles limits the practical use of his formula to Mach numbers between 1.5 and 4, and to half-cone-angles between 10° and 28°, which covers all ogives likely to be found in practice.

8. Though the assumption of the linear variation of $\Delta p/q_1$ with the axial distance along the ogive could be subject to argument, comparison of the wave drag values obtained by Miles' formula with results calculated by other methods as well as with experimental data, seems to indicate that within the limitations stated by Miles, the formula given by him is sufficiently accurate for most practical purposes.

9. Another way of determining the pressure distribution on the ogival nose is to use the method presented by the author in reference (a). It is based on the fact, noted by Fowler and French in reference (d), that conditions along an ogival nose can be approximated by taking the conditions at the point in question to be the same as those along a cone which is tangent to the ogive at that point, and determining the pressure by the Taylor-Maccoll method of reference (c). Reference (a) presents a complete set of curves enabling one to determine the pressure ratio p_3/p_1 as a function of the tangent cone angle. These curves are based on experimental data and values calculated by the method of characteristics, but the methods of correlation and extrapolation took into account the form of variation of the pressure ratio as a function of Mach number and cone angle, as computed by the Taylor-Maccoll theory. A typical pressure distribution on a 14-caliber ogive determined by the method of reference (a) is shown in Figure 1 of the present report.

10. Because it is more closely related to the actual experimental data, this method should prove to be more accurate than the one previously described, except perhaps for ogives of high fineness ratio at low Mach numbers. So far, all checks against other experimental data as well as results computed by the method of characteristics indicate a very satisfactory correlation in the range of Mach numbers between 1.5 and 5. Not enough data are available to check the method at higher Mach numbers.

11. A third method of getting the pressure distribution around the ogival nose is based on the hypersonic similarity rule, which states that for hypersonic flow about slender, pointed, similarly shaped bodies* of different fineness ratios, the pressure distribution depends only on the similarity parameter K, which is the ratio of the Mach number to the fineness ratio L/D. Enounced first by H. S. Tsien in reference (e), this rule was later found to be applicable to a wide range of Mach numbers, even in the low supersonic range. (See in particular references (f) and (g)). The hypersonic similarity rule applies to rotational flow, and therefore the pressure distributions with rotation effects included are a function of the similarity parameter K only. This result has been specifically demonstrated for the case of the cylindro-ogival body. The influence of rotation, due to the existence of an entropy gradient normal to the streamlines, has been discussed in reference (g). The error in drag due to neglecting rotation increases rapidly with the similarity parameter K, being negligible at K = 0.5, but amounting to about 30% of the total drag at K = 2 (reference (g)). For our present AAP missile, K is equal to 0.375 at a Mach number of 1.5 and 1.125 at M = 4.5. The contribution of rotation at M = 1.5 is therefore negligible, but may be of the order of 10% of the total wave drag at M = 4.5.

*Similarly shaped bodies are defined as those having the same thickness distribution along the length.

12. The hypersonic similarity rule represents a powerful instrument for the calculation of pressure distributions. It actually implies that, if the pressure distribution or drag is known for a given body, the same is known for all similarly shaped bodies having the same value of the similarity parameter. References (f) and (g) indicate how this similarity rule can be used to calculate the pressure on the ogival nose as a function of the similarity parameter K and of the axial distance from the nose tip. Hence, one may obtain the curves presented in Figure 2 of this report and reproduced from Figure 8(a) of reference (g).

13. The similarity method, taking the rotational effect systematically into account, should prove the most accurate of the three methods at high Mach numbers. It is not applicable, however, in the low Mach number range. Its range of applicability has been plotted as a function of the fineness ratio of the ogive in reference (g). It can, however, be grossly expressed thus: the hypersonic similarity rule can be applied to any ogive with a fineness ratio larger than 2.5 and for Mach numbers larger than 2. As the fineness ratio of the ogival nose of the AAP, (being equal to its axial length expressed in calibers), is equal to 4, the wave drag can be computed by the similarity rule for any Mach number above 2.

Determination of the Wave Drag from the Pressure Distribution

14. Consider on the ogival nose of the missile (Figure 3) a very thin annulus limited by two neighboring parallels. On that annulus, two neighboring meridians will determine with the parallels a small elemental area. If dc is the length of the element along the parallels, and dm its length along the meridians, the elemental area is equal to dm.dc. The pressure exerted on this element has a component p_x in the direction of motion (see Figure 4) and if ϕ is the angle of the elemental surface with the direction of motion, the drag component on the elemental area is

$$dD = p \cdot \sin\phi \cdot dm \cdot dc.$$

If the radii of the parallels delimiting the annulus are r and r + dr respectively, the following relationship holds (see Figure 5):

$$dr = dm \cdot \sin\phi .$$

Therefore: $dD = p \cdot dc \cdot dr$, and the total wave drag, D_W, on the ogive is given by:

$$D_W = \int_0^R \int_0^{2\pi r} (p \cdot dr)\, dc = \int_0^R 2\pi r \cdot p \cdot dr = \pi \int_0^{r=R} p\, d(r^2),$$

where R is the maximum radius of the ogive.

It can be seen, therefore, that if r^2 is plotted on a graph in abscissae and the corresponding value of the surface pressure is plotted in ordinates, the value of the wave drag may be obtained from a determination of the area under the curve. In practice the surface pressure is given in the form p_s/p_1 or in a similar form, $(p_s-p_1) / p_1$, where p_s is the surface pressure and p_1 the pressure of the undisturbed stream. The radius r is given by the function representing the ogival contour, i.e.:

$$r = y = -(N_c - \tfrac{1}{2}) + \sqrt{N_c^2 - (x - \sqrt{N_c - \tfrac{1}{4}})^2},$$

where N_c is the caliber number of the ogive, and x and y the coordinates of one of its points expressed in calibers. If the tangent cone angle method is used, the procedure is then the following: several values of x are chosen so as to cover the axial length of the ogive with equal intervals. For each value of x, the corresponding value of the equivalent half-cone-angle θ is obtained either from the tables of reference (a) or from the equation:

$$\tan \theta = \frac{\sqrt{N_c - \tfrac{1}{4}} - x}{\sqrt{N_c^2 - (x - \sqrt{N_c - \tfrac{1}{4}})^2}} .$$

For each value of θ thus obtained, a value of the pressure ratio p_s/p_1 can be determined from the curves of reference (a). Also for each value of x selected, a value of y and of y^2 is obtained, and p_s/p_1 is plotted against y^2. The procedure is analogous if the similarity method is used, and in both cases a curve of the shape illustrated in Figure 6 is obtained. It will be observed that a partial vacuum exists near the junction of the ogive with the cylinder. As only a surface pressure above that of the free stream can contribute positively to the wave drag, the procedure will then be to measure the area ABCDA and subtract from it the area of the rectangle CDEF. The value of the integral multiplied by πp_1 will then give the value of the wave drag.

Numerical Results for the Wave Drag Coefficient

15. Calculations for the AAP were made using the tangent cone method to obtain the pressure distribution, and measuring the areas with a planimeter. The results obtained for the wave drag coefficient C_{D_W} are as follows:

Table I

Wave Drag Coefficient at Wind-Tunnel Mach Numbers

M	1.86	2.5	3.24	4.5
C_{D_W}	0.051	0.051	0.048	0.048

This coefficient is referred to the maximum diameter of the ogive, i.e., the diameter of the tangent cylinder. The skin friction and the base drag coefficients will be referred to the same area. Being independent of the air density and of the Reynolds number, the above results are valid for full-scale free-flight tests as well as for wind-tunnel and aerodynamic range tests.

The Skin Friction Coefficient

16. For the sake of simplification, skin friction analyses are usually made by assuming that the missile is replaced by a flat plate of the same over-all length. We shall consider separately the cases of the laminar and the turbulent boundary layers.

Laminar Skin Friction

17. The laminar skin friction on a flat plate can be obtained by the following simple formula, presented on page 8 of reference (n):

$$C_f\sqrt{R_e} = 1.328 - 0.0217\ M^{3/2},$$

where C_f is the skin friction coefficient referred to the unit area of wetted skin. The skin friction is affected by a change of scale or a change in density conditions. The present numerical calculation will refer to wind-tunnel tests only.

18. The length of model used in wind-tunnel testing was 13 in. The Reynolds number per foot of model, and hence the Reynolds number for the model, are given by the following table, the Mach numbers being those of wind-tunnel tests:

M	1.86	2.5	3.24	4.5
Re (millions) per foot	4.10	3.10	2.20	1.20
Re for model	4.44	3.36	2.38	1.30

In order to convert the skin friction coefficient into a drag coefficient referred to the cylindrical cross section, it is necessary to know the area of the ogival nose.

Determination of the Ogival Nose Area

19. The surface area, A, of any body of revolution of axial length L is given by:

$$A = 2\pi\int_0^L y\sqrt{1+(dy/dx)^2}\ dx\ .$$

In the case of the ogive, we have

$$y = -(N_c - \tfrac{1}{2}) + \sqrt{N_c^2 - \left(x - \sqrt{N_c - \tfrac{1}{4}}\right)^2} \quad \text{and} \quad \frac{dy}{dx} = \frac{\sqrt{N_c - \tfrac{1}{4}} - x}{\sqrt{N_c^2 - \left(x - \sqrt{N_c - \tfrac{1}{4}}\right)^2}} .$$

As shown by Charles J. Kulishek, the integral has a simple analytical solution.

Let $L = \sqrt{N_c - \tfrac{1}{4}}$ and $b = -(N_c - \tfrac{1}{2})$. Then:

$$A = 2\pi \int_0^L \left[b + \sqrt{N_c^2 - (x-L)^2} \right] \left[\sqrt{1 + \frac{(L-x)^2}{N_c^2 - (x-L)^2}} \right] dx ,$$

$$A = 2\pi b N_c \int_0^L \frac{dx}{\sqrt{N_c^2 - (x-L)^2}} + 2\pi N_c \int_0^L dx ,$$

$$A = 2\pi b N_c \left[\sin^{-1}\left(\frac{x-L}{N_c}\right) \right]_0^L + 2\pi N_c (x)_0^L ,$$

$$A = 2\pi b N_c \left[\sin^{-1}\left(\frac{L}{N_c}\right) \right] + 2\pi N_c L .$$

For a 16.25 caliber ogive, it was found that the surface area is 8.465 square-calibers, i.e., 8.465 D^2, where D is the maximum cross-sectional diameter of the ogive.

20. The cylindrical portion of the body being 6 calibers long, its surface area will be 6π square-calibers. The total area of the ogive-plus-cylinder is then 27.315 square-calibers. The maximum cross-sectional area of the missile to which the various drag coefficients are referred is $\pi/4$ square-calibers. The ratio of the wetted area to the cross-sectional area is then 34.778, which is the factor by which the skin friction factor C_f should be multiplied in order to get the skin friction drag coefficient, $C_{D_{S.F.}}$.

The latter is given in the table below:

TABLE II

Laminar Skin Friction Drag Coefficient at Wind-Tunnel Mach Numbers

M	1.86	2.5	3.24	4.5
$C_{D_{S.F.}}$	0.021	0.024	0.027	0.034

Turbulent Skin Friction

21. The case of the turbulent boundary layer lends itself to a considerably less reliable analysis than the laminar case, and the numerical results obtained by various theoretical analysts differ considerably. This is, of course, mainly due to the fact that not only the real nature of turbulence is unknown, but no successful model describing this phenomenon has been presented. Among the various analyses available, some, like Van Driest's and Ferrari's, assume with Prandtl that the mixing length l is proportional to the distance y along a direction normal to the surface of the missile; others (Frankl and Voishel, Wilson, etc.) assume with von Karman that l is proportional to $(du/dy)/(d^2u/dy^2)$, where u should be taken as the component of the free-stream velocity parallel to the surface of the missile, at a given distance from the nose. The methods also differ from each other in the way compressibility is taken into account, and in the mathematical approximations used. A critical review of these various analyses has been made in the excellent report of Morris Rubesin and his co-workers (reference (h)) which includes a representative bibliography. Therefore only the major conclusions that may be derived from this study will be presented here.

22. In the analysis made by Frankl and Voishel, the limiting case for M = 0 leads to the formula derived by Schlichting:

$$C_f = \frac{0.472}{(\log_{10} Re)^{2.58}},$$

where Re is the Reynolds number of the undisturbed stream. The other analyses do not lead to the same limiting value, but, for comparison's sake, it is convenient to refer all the results to the Schlichting equation, which yields the following numerical values:

Table III

Schlichting's Friction Drag Coefficient at Wind-Tunnel Mach Numbers

M	1.86	2.5	3.24	4.5
$C_{D_{S.F.}}$	0.124	0.130	0.138	0.154

23. From the results calculated by Rubesin, the author constructed the following table giving the value of $C_f/(C_f)_{M=0}$, (where the denominator represents the Schlichting value), for Mach numbers between 1 and 4, and for several representative analyses made. The entry of the last line,

labelled "Extended Frankl-Voishel Analysis", follows the nomenclature used in reference (h). This analysis, however, was made by Rubesin, along the lines indicated by Frankl, but assuming a linear variation of viscosity with temperature, and solving the momentum integral numerically to avoid certain simplifications made by Frankl which would have reduced the applicability of the method to the range of low supersonic Mach numbers.

Table IV

Ratio of Friction Drag Coefficients Calculated by Various Theories to the Schlichting Value for M = 0

Mach Number	1	1.5	2	2.5	3	3.5	4
Van Driest	0.950	0.900	0.845	0.780	0.735	0.680	0.650
Wilson	0.930	0.860	0.790	0.725	0.660	0.600	0.560
Extended F-V	0.925	0.845	0.760	0.690	0.625	0.560	0.515

The comparison between these analyses is also represented graphically in Figure 7. It is seen that, at a Mach number of the order of 4, the discrepancy between the numerical results of the three methods mentioned here is fairly high.

24. The various theoretical analyses were compared by Rubesin with available experimental data. It appears that within the range of Mach numbers and Reynolds numbers presently considered, the extended Frankl-Voishel theory predicts the skin friction coefficient better than the others. The accuracy is better than 5% at Mach numbers up to 2.5. In general the agreement between theory and experiment would seem to be very good, but a comparison of a typical experimental boundary-layer velocity distribution with a similar distribution calculated by Rubesin according to the Frankl-Voishel extended analysis revealed that the velocity profiles were not coincident. A similar study made by Wilson, following his own analysis of the boundary layer, showed a similar discrepancy in the profiles (reference (i)). This seems to indicate that, as far as the skin friction coefficient is concerned, the agreement between theory and experiment may be fortuitous, and that none of the present theories should be considered wholly reliable.

25. From comparisons between predicted and experimental values of the drag coefficient, the author arrived to conclusions similar to those of Rubesin, and consequently the extended Frankl-Voishel analysis was used in the present study. Advantage was taken of the interpolation formula derived by Rubesin and given below:

$$C_f = \frac{0.472}{(\log_{10} Re)^{2.58} \cdot \left(1 + \frac{\gamma-1}{2} M_e^2\right)^{0.467}} ,$$

where Re and Mo are the Reynolds number and the Mach number related to the free-stream conditions. This formula represents the results computed numerically to within ± 2% in the range $0 < M_o < 4$.

26. The value of the turbulent skin friction drag coefficient corresponding to the wind-tunnel tests of the AAP is then given by the table below:

Table V

Estimated Turbulent Skin Friction Drag Coefficient at Wind-Tunnel Mach Numbers (Extended Frankl-Voishel Method)

M	1.86	2.5	3.24	4.5
$C_{D_{S.F.}}$	0.0970	0.0891	0.0814	0.0720

27. Using the results of Figure 7, the following table, giving the turbulent skin friction drag coefficients obtained by various methods can be computed:

Table VI

Turbulent Skin Friction Drag Coefficients Calculated by Various Methods

M	1.86	2.5	3.24	4.5
Schlichting for M = 0	0.1240	0.1300	0.1380	0.1540
Van Driest	0.1066	0.1015	0.0978	0.0949
Wilson	0.1005	0.0942	0.0872	0.0770
Ext. F-V	0.0970	0.0891	0.0814	0.0720

Mixed Boundary Layers

28. Having determined the skin friction drag coefficient for turbulent boundary layers at the various Mach numbers occurring in the wind tunnel, the next problem is to predict the nature of the boundary layer as a function of the nozzle Mach number. This problem cannot at present be solved analytically, and we have to base our estimated guess on the observation of a number of wind-tunnel schlieren photographs. Though the determination of the nature of the boundary layer from a schlieren picture is by no means always precise, it appears that, at a Mach number of 1.86, the ogival head only is in laminar flow, while at Mach numbers of 2.5 and

higher, the boundary layer is laminar over the whole model. If part of the boundary layer only is laminar, calling C_1 and C_2 the skin friction drag coefficients for the laminar and turbulent boundary layers respectively, the total $C_{D_{S.F.}}$ for the model will be:

$$C_{D_{S.F.}} = \frac{k_1 C_1 + k_2 C_2}{k_1 + k_2},$$

where k_1 and k_2 are the areas of the body wetted by a laminar and turbulent boundary layer, respectively. If the laminar flow is localized to the ogive, we have: $k_1 = 8.465$ and $k_2 = 18.850$. Hence the following table which gives our estimated values of the skin friction drag coefficient:

Table VII

Final Estimated Values of the Skin Friction Drag Coefficient at Wind-Tunnel Mach Numbers

M	1.86	2.50	3.24	4.50
$C_{D_{S.F.}}$	0.073	0.024	0.027	0.034

The variation of the skin friction drag coefficients calculated in this chapter has been plotted as a function of the Mach number in Figure 8.

Base Drag

29. The component of the drag which is the most difficult to evaluate is, without much doubt, the base pressure drag. No analytical evaluation of this drag has been made yet, even in a simplified form. The Reynolds number effect on the base drag is very important insofar as it affects the boundary layer, but so are the influences of a variation of the velocity or the temperature distributions. A correct prediction of base-pressure values requires a full knowledge of the boundary-layer profiles.

30. The base drag coefficient, C_{D_B}, is given by:

$$C_{D_B} = \frac{2(1 - p_b/p_1)}{\gamma M^2},$$

where p_b is the base pressure, p_1 the pressure of the undisturbed stream, and M the free-stream Mach number. It is therefore necessary to know the value of p_b/p_1 for a given missile as a function of the Mach number and Reynolds number in order to determine its base drag.

31. Fortunately, certain simplifications can be made. The experimental results presently available seem to indicate that the head shape has little influence over the base pressure. Dr. A. C. Charters remarks that the flows over conical heads with slightly different cone angles should reach about the same condition over the body. When the cone angle at the nose tip is decreased, the head pressure is also decreased, but at the same time the drop in pressure around the shoulder to the body is decreased, and the two should tend to cancel. By application of the tangent cone method presented in reference (a), similar considerations may be applied to the ogive. The interference between head and base seems to become worthy of consideration only when the length of the attached cylinder is of the order of one caliber or less (see reference (j)). It can therefore be inferred that, at least in first approximation, all square-based missiles of about the same over-all length, tested under the same atmospheric conditions and at the same Mach number, will have the same base drag coefficient.

32. Some conclusions on the Reynolds number effect on base pressures were drawn by the author from a study of base pressure measurements by Dr. H. H. Kurzweg (references (k) and (l)). From his results the following table may be drawn.

Table VIII

p_b/p_1 Values Obtained by H. H. Kurzweg in NOL Wind-Tunnel Tests

Reynolds number in millions	1	2	3	4	5
M = 1.56	0.50	0.61	0.67	0.68	-
M = 1.86	0.45	0.56	0.61	0.62	-
M = 2.48	0.45	0.46	0.45	0.50	0.52
M = 2.87	0.50	0.42	0.39	0.41	-
M = 3.24	0.62	0.47	0.39	-	-

The reader is reminded that the Reynolds number of the model at the various Mach numbers corresponding to the wind-tunnel tests of the AAP may be found in paragraph 18.

33. The results of Table VIII are plotted in Figures 9 and 10. It may be seen that the curves giving the pressure ratio p_b/p_1 as a function of the Mach number first decrease almost linearly, reach a minimum and increase again toward an asymptotic value. At low Mach numbers (below three), the curves corresponding to Reynolds numbers of three million and above are

almost perfect straight lines, but the curve corresponding to a Reynolds number of one million already presents a minimum at a Mach number of the order of 2. As the Reynolds number increases, the minimum value of the curve seems to shift slightly toward higher Mach numbers. It is unfortunate that no information is available on base pressures in the ranges of high Mach numbers and Reynolds numbers to confirm this hypothesis. At present, the portions of the curves above a Mach number of 3.25 are no more than plausible guesses, but their general shape is probably correct.

34. The shape of the curves presented in Figure 10 may explain certain discrepancies between test values of the base pressures obtained in different wind tunnels, and also between wind-tunnel and free-flight values. It may be seen that the pressure-ratio curves for Reynolds numbers of one and two million are fairly wide apart. At a Mach number below two for instance, the curve for $Re = 10^6$ will give a much lower value of the pressure ratio than the curve $Re = 2.10^6$, but the reverse is true at a Mach number of three and above. The wind-tunnel Reynolds number is therefore an important consideration. On the other hand, at large values of the Reynolds number, the curves get very close together, and, as far as full-scale missiles are concerned, even a substantial change in the length of the body should not affect the base pressure, unless very high altitudes are reached. The assumption made by Dr. Charters in reference (m) that the base pressure is independent of the Reynolds number is probably quite satisfactory at high Reynolds numbers, but the same assumption used in the interpretation of wind-tunnel data and in correlation between such data and full-scale tests would be erroneous.

35. From the curves presented in Figure 10, extrapolated when necessary, the following table was obtained:

Table IX

Base Drag Coefficient vs Wind-Tunnel Test Mach Number

M	1.86	2.5	3.24	4.5
C_{D_B}	0.151	0.123	0.076	0.015

Total Body-Drag Coefficient

36. Now that the three basic components of the body-drag coefficient have been estimated, the following table may be set up:

Table X

Body-Drag Components and Total Body-Drag vs. Mach Number. Comparison with Wind-Tunnel Data.

M	1.86	2.5	3.24	4.5
Estimated C_{D_W}	0.051	0.051	0.048	0.048
Estimated $C_{D_{S.F.}}$	0.073	0.024	0.027	0.034
Estimated C_{D_B}	0.151	0.123	0.076	0.015
Estimated body-drag coefficient C_D	0.275	0.198	0.151	0.097
C_D obtained in NOL wind-tunnel tests	0.265	0.200	0.145	$\approx$ 0.080

The variation of the drag components with the Mach number is illustrated in Figure 17. Over the range of Mach numbers considered, the wave drag coefficient remains practically constant. The skin friction coefficient varies substantially only in the region of transition, when a turbulent boundary layer begins to appear on the cylindrical portion of the model. The variation of the base pressure drag coefficient parallels that of the total body-drag coefficient, and below M = 3.5, the base pressure drag is by far the most significant factor.

Accuracy of the Estimated Components of the Body-Drag Coefficient

37. If u, v, w and y represent the wave, skin friction, base and total body-drag coefficients respectively, and if r_u, r_v, r_w, and R are their respective probable errors, then

$$y = u + v + w, \quad \text{and}$$

$$R^2 = \left(\frac{\partial y}{\partial u}\right)^2 r_u^2 + \left(\frac{\partial y}{\partial v}\right)^2 r_v^2 + \left(\frac{\partial y}{\partial w}\right)^2 r_w^2, \quad \text{or}$$

$$R = \sqrt{r_u^2 + r_v^2 + r_w^2}.$$

The probable error in the computed values of the wave drag should be less than 1%, and could, if necessary, be reduced by computing the pressure distributions analytically. It should not exceed $\pm$ 0.001 within the range of Mach numbers considered here. At Mach numbers of 2.5 and above, when the boundary layer is fully laminar, the probable error in the skin friction coefficient should not exceed $\pm$ 5%, and it is possible again to take r_v = 0.001. At Mach numbers below 2.5, the uncertainty becomes greater, because the value of the skin friction for a turbulent boundary layer is not known as

well as for a laminar boundary layer, and because the position of the transition point is itself subject to a rough approximation. This is compensated to some extent by the fact that the base pressure coefficient is best known in this range of Mach numbers. The estimates of the probable errors in the components and the resulting value for the total body-drag coefficient are presented in Table XI. The body drag at a Mach number of 1.86, for example, should then read: 0.275 $\pm$ 0.011.

Table XI

Estimated Errors on the Body-Drag Components and Resulting Error in the Computed Value of the Total Body Drag

M	1.86	2.5	3.24	4.5
r_u	0.001	0.001	0.001	0.001
r_v	0.009	0.004	0.001	0.001
r_w	0.009	0.009	0.009	0.014
R	0.013	0.010	0.009	0.014
R as % of C_D	4.7	5.0	6.0	14.5

38. As may be seen from the above table, there is relatively little change in the absolute value of the error in the drag coefficient over the Mach number range considered. On the other hand, the relative error may vary from $\pm$ 5% to $\pm$ 15% of the estimated drag coefficient. The importance of obtaining more experimental data on the base pressure drag at high Mach numbers under various Reynolds number conditions is obvious.

Comparison with Experimental Results

39. The curves of the estimated and measured wind-tunnel body drag are shown in Figure 11. It can be seen that the correlation is excellent at the lower Mach numbers, and fairly good even at a Mach number of 4.5. At this Mach number, due to a poor knowledge of the base drag, the probable error on the estimated result becomes fairly large. It happens in this particular case that the absolute value of the probable error on the estimated result is almost equal to the difference between the estimated and the experimental value. But this might well be simply coincidental. At high Mach numbers especially, the accuracy of wind-tunnel drag measurements is doubtful, and such experimental results cannot be used to determine the accuracy of the present method of prediction.

PART II

Drag Due to the Addition of Fins

40. The addition of the fins affects the total drag in several ways. The fins have a wave drag of their own, contribute to the skin friction and modify the base drag in two different ways:

a. Because of a change in the flow pattern at the rear of the body and in the wake, the base pressure will be different from the case of the body without fins.

b. The base of the fins contributes an increase of base area as compared to the case of the body alone.

On the other hand, for the case of zero angle of incidence as treated in this Report, there is no cross-flow effect to be considered.

41. The original configuration of the finned body of the AAP, as used in NOL wind-tunnel tests, is shown in Figure 12. Note that the over-all diameter is twice the diameter of the body alone. The fin thickness was originally 0.375 in. For the wind-tunnel tests, the fin thickness was 0.1096 in. and the body diameter was 1.3 in.

42. The problem of wave drag of a flat plate with beveled edges has not yet been solved analytically, but it was considered satisfactory as a first approximation to replace the beveled-edged flat plate by a symmetrical double-wedge airfoil section, the drag of which has been determined analytically. The fin configuration was redesigned as shown in Figure 13.

43. The present calculations follow the method of reference (o) which is based on the linearized supersonic theory and assumes that the shock waves are sufficiently weak to be approximated by Mach waves. Further restrictions defining the class of wings to which the charts of reference (o) apply are as follows:

a. The wings are symmetrical about an axis in the direction of the free stream;

b. the wings are of hexagonal planform;

c. the leading edges are swept back;

d. the side edges are parallel to the free stream; and

e. the airfoil section is polygonal and symmetric about the plane of the wing.

The restrictions listed above limit the attitude to nonyawed positions.

44. The wave drag coefficient at zero lift, C_{D_W}, is given by the sum of the wave drag coefficients resulting from the thickness distribution, C_{D_b}, and from the camber distribution, C_{D_c}, that is

$$C_{D_W} = C_{D_b} + C_{D_c}.$$

Since the fin profile as shown in Figure 13 is symmetrical about the chord line, the wave drag due to camber distribution will be zero and therefore the total wave drag coefficient at zero lift will be the wave drag coefficient which results from thickness distribution.

45. As shown by Ellis Lapin in reference (o), the wave drag coefficient C_{D_b}, due to thickness distribution, may be computed in the form $\beta C_{D_b}/\mu^2$, where μ is the local slope of the wing surface of an uncambered wing, and β is equal to $\sqrt{M^2-1}$, where M is the Mach number. The coefficient $\beta C_{D_b}/\mu^2$ is computed by considering it to be composed of two parts: the principal part is $\beta C_{D_{b_0}}/\mu^2$ which represents the drag coefficient at zero lift. To this is added an incremental correction $\beta \Delta_1 C_{D_b}/\mu^2$ which is the incremental drag coefficient at zero lift induced by the presence of side edges. In addition, another correction $\beta \Delta_2 C_{D_b}/\mu \Delta \mu$ must be added to account for the influence of a subsonic rear edge. This correction is dependent upon the change in surface slope when proceeding from one element to the succeeding element. The charts presented in the above-mentioned reference give $\beta C_{D_b}/\mu^2$ and the two incremental corrections as functions of the planform parameters m, m_t/m and a_t/m. These parameters are defined as follows:

m = ratio of the slope of the leading edge to the Mach line slope;

m_t = ratio of the slope of the trailing edge to the Mach line slope;

a_t = ratio of the slope of a ray connecting the fin leading edge vertex and the tip trailing edge to the Mach line slope.

Numerical Computations of Planform Parameters and C_{D_b}

46. The fin profile is divided into elements (I and II as shown in Figure 13) from which the planform parameters are determined:

ELEMENT I

$$\frac{m_t}{m} = \frac{\frac{s}{b_1}}{\frac{s}{b_1}} = 1$$

$$\frac{a_t}{m} = \frac{\frac{s}{(b_1+h)}}{\frac{s}{b_1}} = 0.8038$$

The quantities s, b, and h are shown graphically in Figure 13 and defined in the list of symbols found at the end of this Report.

The parameter m is given by the expression

$$m = \frac{\frac{s}{b}}{\frac{1}{\sqrt{M^2-1}}} = \frac{\frac{0.5d}{1.5d}}{\frac{1}{\sqrt{M^2-1}}} = \frac{\sqrt{M^2-1}}{3},$$

where M is the Mach number.

Therefore the basic drag coefficient and the two incremental corrections may be found from the charts of reference (o), using the above-defined parameters.

47. A sample computation of the wave drag coefficient, C_{D_b}, for Element I at Mach number 3.24 is shown:

From the charts of reference (o), the coefficient $\beta C_{D_{b_o}}/\mu^2$ at zero lift and the incremental drag coefficient $\beta \Delta_1 C_{D_b}/\mu^2$, are then given as follows:

Table XII

Intermediate Coefficients for Fin Drag Calculations

a_t/m	$\beta C_{D_{b_o}}/\mu^2$	$\beta \Delta C_{D_b}/\mu^2$
0.4	3.29	-0.319
0.6	3.98	-0.140
0.8	5.50	-0.053

48. Since $m\beta > 1$, that is to say, the leading edge slope is greater than the Mach line slope, and $m = m_t$, the incremental drag coefficient correction $\beta \Delta_2 C_{D_b}/\mu\Delta\mu$, which accounts for the influence of a subsonic rear edge, is zero.

At Mach 3.24, when $a_t/m = 0.8038$,
$\beta C_{D_b}/\mu^2 = 5.501$
$\beta \Delta_1 C_{D_b}/\mu^2 = -0.054$.

49. The wave drag coefficient of four fins with respect to the body cross-sectional area is found to be:

$$C_{D_b} = \frac{(5.501-0.054)(0.1151)^2}{3.0818} \cdot \frac{A_{BE}}{\pi/4} \cdot 4,$$

where A_{BE} is the area of the beveled edge projected on the chord line, whose sides are a and h and whose included angle is γ. The area is expressed as follows:

$$A_{BE} = a.h.\sin\gamma$$

$$= 1.5811 \times 0.3662 \sin 18.43°$$

$$A_{BE} = 0.1831 \text{ square-calibers.}$$

Therefore:

$$C_{D_b} = \left[\frac{5.447 \times (0.1151)^2}{3.0818}\right] \cdot \left[\frac{0.1831 \times 16}{3.1416}\right],$$

$$C_{D_b} = 0.0218.$$

50. It will be observed that the wave drag at an angle of zero lift of the AAP fin will be the airwise force resulting from the pressure distribution on the beveled edge only; the flat plate element will contribute nothing to the pressure drag. Therefore, the wave drag of the AAP fins will be represented by the wave drag of the beveled edge (Element I in Figure 13), the drag contribution of Element II being neglected. The following chart shows the results of the above method of computation, the wave drag coefficient for the four fins being referred to the body cross-sectional area.

Table XIII

Fin Wave Drag Coefficient vs Mach Number (by Lapin's Method)

Mach No.	Fin Wave Drag Coefficient C_{D_W} (Four Fins)
1.86	0.0363
2.50	0.0286
3.24	0.0218
4.50	0.0139

51. In the above calculations, the Mach number value should be taken not in the undisturbed stream but in the immediate vicinity of the leading edge of the fin. The local Mach number at the fin edge can be easily determined if it is assumed that the static pressure p_3 before the shock produced by the fin is equal to the free-stream static pressure.

52. The computation of local Mach numbers was made for free-stream Mach numbers of 1.80, 2.00, 3.00, 4.00 and 5.00. Knowing the angle of flow deflection at the nose of the missile (which is equal to the half-nose angle), the shock angle may be obtained from Figure 8 of reference (p). Knowing the shock angle, from Figure 3 of reference (p), one can obtain the total pressure ratio p_{o3}/p_{o1}, where p_{o3} is the stagnation pressure before the shock produced by the fins and p_{o1} is the stagnation pressure before the shock produced by the missile nose. Assuming isentropic flow behind the shock waves, the pressure ratio p_1/p_{o1}, (where p_1 is the free-stream static pressure), is obtained for each free-stream Mach number from reference (q). The ratio p_3/p_{o3} may then be computed. We have:

$$\frac{p_1}{p_{o3}} = \frac{p_1}{p_{o1}} \times \frac{p_{o1}}{p_{o3}},$$

in which p_1/p_{o1} and p_{o3}/p_{o1} were calculated previously. As it was assumed that $p_1 = p_3$, the ratio p_3/p_{o3} is known. To this ratio corresponds a certain local Mach number which, if isentropic expansion is assumed, may be obtained from the tables of reference (q).

53. The results of the above calculations are presented in Table XIV.

Table XIV

Local Mach Number at the Fin Leading Edge
vs Free-Stream Mach Number

Free-Stream Mach No.	Local Mach No. at Fin Leading Edge
1.80	1.80
2.00	1.99
3.00	2.99
4.00	3.95
5.00	4.88

It may be seen that, except at the higher Mach numbers, the difference between free-stream and local Mach number is small, and, as a first approximation, the free-stream Mach number may be assumed at the leading edge of the fin.

54. An approximation to the wave drag produced by the fins may be obtained by another method, suggested by Sidney Fagin. As previously noted in this report, the wave drag at an angle of zero lift will be the airwise force resulting from the pressure distribution on the beveled edge only. Omitting the skin friction drag (calculated later in this report), the fin drag coefficient may be expressed as the sum of the wave drag coefficient, C_{D_W}, and the base drag coefficient, C_{D_B}, where

$$C_{D_W} = \frac{2(p_2 - p_3).t.s}{q_1.A_c} \quad \text{(per fin), and}$$

$$C_{D_B} = \frac{2(p_3 - p_{bf}).t.s}{q_1.A_c} \quad \text{(per fin), where}$$

s = fin semi-span;

t = fin semi-thickness;

p_{bf} = static pressure at the base of the fin;

p_2 = static pressure behind the shock;

p_3 = static pressure in front of the shock;

q_1 = free-stream dynamic pressure = $\frac{\gamma}{2} p_1.M_1^2$;

A_c = body cross-sectional area (see Figures 14 and 15).

Then, excluding skin friction, the fin drag coefficient per fin may be represented by the expression:

$$C_D = \frac{2(p_2-p_3).t.s}{q_1.A_c} + \frac{2(p_3-p_{bf}).t.s}{q_1.A_c} .$$

In order to use the above equation, the base pressure at the rear of the fin must be estimated. An upper value of the fin drag coefficient is obtained when $p_{bf} = 0$. Then, for each fin,

$$C_D = \frac{2\ p_2.t.s}{q_1.A_c} = \frac{2\ p_2.t.s}{q_3.A_c}\left(\frac{q_3}{q_1}\right) = \left(\frac{p_2/p_3}{q_3/p_3}\right)\left(\frac{q_3}{q_1}\right) \cdot \frac{2\ t.s}{A_c} .$$

Therefore, in order to compute the fin drag coefficient, it is necessary to determine the ratios p_2/p_3, q_3/p_3 and q_3/q_1 as functions of the free-stream Mach number.

55. The shock angle α (see Figure 14) can be determined as a function of the free-stream Mach number and the flow deflection angle (half-cone angle) from the Oblique Shock Tables of reference (q). The normal component of the Mach number in front of the shock is then equal to $M_3 \cdot \sin\alpha$, and the corresponding values of p_2/p_3 are found from the Normal Shock Tables for $\gamma = 1.4$ in reference (q) (under the column heading p_2/p_1). Similarly, the ratio q_3/p_3 is found from the Isentropic Tables of reference (q) for given values of M_3 (under the column heading q/p). Finally, the ratio q_3/q_1 may be determined in the following manner: knowing the free-stream Mach number M_1 and the Mach number M_3 at the leading edge of the fin, the pressure ratios q_1/p_1 and q_3/p_1 may be obtained from the Isentropic Flow Tables of reference (q) (under the column heading q/p). Hence q_3/q_1 is readily obtained as a function of the free-stream Mach number, and finally C_D may be calculated.

56. The values of the drag coefficient, referred to the body cross-sectional area (excluding skin friction), as calculated by the above method, are presented in Table XV below:

Table XV

Total Fin Drag Coefficient vs Free-Stream Mach Number (By the Static Pressure Assumption Method)

Free-Stream Mach No.	Total Fin Drag Coefficient, Four Fins
1.86	0.123
2.50	0.076
3.24	0.049
4.50	0.030

It should be remembered that these values are only upper limits of the total fin wave drag coefficient, excluding skin friction. Further investigations of this point are necessary and will be made, but at present the author doubts that the above method would provide enough accuracy for practical purposes, unless some fairly good assumptions on the value of the fin base pressure can be made.

Fin Skin Friction

57. The total longitudinal length of a fin in the original wind-tunnel models of the AAP was equal to 3 calibers, or 0.325 ft. The reader is reminded that the Reynolds number per foot of model in the NOL wind tunnels varies from 4.1 million at M = 1.86 to 1.2 million at M = 4.5. Furthermore, the air velocity at the fin is smaller than the velocity of the undisturbed stream. Hence, except perhaps at the lowest Mach number, the flow along the fin will be almost entirely laminar, and use may be made of the equation presented in paragraph 16:

$$C_f \sqrt{Re} = 1.328 - 0.0217\, M^{3/2},$$

where C_f is the skin friction factor referred to the unit area of the wetted surface of the fin.

58. To obtain the fin skin friction drag coefficient, it is necessary to know the ratio of the total wetted area of the four fins to the cross-sectional area of the body. The wetted surface of a fin consists of two beveled edges, two planforms and the fin tip. The area ratio was found to be equal to 16.10, which is the quantity by which the fin skin friction factor must be multiplied in order to obtain the fin skin friction coefficient. Hence, the following table may be obtained:

Table XVI

Fin Skin Friction Drag Coefficient
vs. Mach Number

Free-Stream Mach No.	Skin Friction Factor (per unit of wetted area)	Fin Skin Friction Drag Coefficient, Four Fins
1.86	0.00110	0.0178
2.50	0.00124	0.0199
3.24	0.00142	0.0229
4.50	0.00179	0.0289

Contributions of the Fins to the Total Base Drag

59. The base pressure for the body alone, as determined in Part I of this Report, will be changed by the presence of the fins, due to changes in the

flow at the rear of the missile and in the wake. This effect does not seem to be presently amenable to an analytical treatment of practical reliability, and about the only source of information on this subject would be a judicious generalization of experimental data. Unfortunately such data are available only for the lower Mach number range, and even in that range are far from plentiful. The ratio of base pressures for a given missile with and without the fins seems to be little dependent upon the exact fin configuration (as long as the general shape remains approximately the same). It varies probably with the number of fins and their spacing. And it certainly is greatly dependent upon the Mach number and the Reynolds number (or more accurately, the characteristic values of the boundary layer near the base).

60. Some interesting values of base pressures on a model of AAP with and without fins were obtained at OAL and communicated to the writer by J. E. Greene. The tests were made at Mach numbers of 1.5, 2.0 and 2.5. In the OAL tunnels, the Reynolds number per inch of model is 5.23×10^5 at M = 1.5, 6.22×10^5 at M = 2.0 and 6.01×10^5 at M = 2.5. The length of the models tested was 10.52 in. and 13.32 in. corresponding to body diameters of 1.30 in. and 1.65 in. respectively. For each Mach number, the tests were therefore made at two different Reynolds numbers. The results obtained are presented in the table below.

Table XVII

Comparison of Base Pressure Coefficients for AAP Model With and Without Fins (OAL Experimental Data)

		M = 1.5		M = 2		M = 2.5	
		Re x 10^{-6}		Re x 10^{-6}		Re x 10^{-6}	
		5.50	6.97	6.54	8.28	6.32	8.00
P_b/P_1	Without fins	0.66	0.97	0.50	0.98	0.40	0.82
	With fins	0.64	0.94	0.45	0.74	0.30	0.70
	Ratio $\frac{\text{with}}{\text{without}}$	0.97	0.97	0.90	0.756	0.75	0.854

Correlating the above results with others obtained in the NOL wind tunnel or determined indirectly from various total drag tests, the approximate curves presented in Figure 16 appear to be the most probable. These curves give the factor by which the base pressure of the body alone should be multiplied to take into account the presence of the four fins.

61. It is then possible to set up the base drag calculations as in the table below, using curve (A) of Figure 16.

Table XVIII

Base Pressure Drag of Finned Configuration

Mach Number	1.86	2.50	3.24	4.50
Re, millions	4.44	3.36	2.38	1.30
p_b/p_1 for bare body	0.634	0.461	0.440	0.786
Correction Factor for fin presence	0.684	0.466	0.472	0.975
p_b/p_1 for finned body	0.434	0.215	0.208	0.766
C_{D_B} for finned body	0.284	0.218	0.131	0.020

62. The following drag breakdown table can then be prepared, and by adding the various drag components, the total drag of the finned body may be plotted.

Table XIX

Drag Breakdown of the Finned Missile at Various Wind-Tunnel Mach Numbers

Mach Number	1.86	2.50	3.24	4.50
C_{D_W} body	0.051	0.051	0.048	0.048
$C_{D_{S.F.}}$ body	0.073	0.024	0.027	0.034
C_{D_B} body + fins	0.284	0.218	0.131	0.020
C_{D_W} fins	0.036	0.029	0.022	0.014
$C_{D_{S.F.}}$ fins	0.018	0.020	0.023	0.029
C_D body + fins TOTAL	0.462	0.342	0.251	0.145
C_D body alone TOTAL	0.275	0.198	0.151	0.097
Ratio C_D Total $\frac{\text{body + fins}}{\text{body alone}}$	1.680	1.727	1.662	1.495

63. The variation of the various drag components, as well as the total drag of the finned missile, as a function of the wind-tunnel Mach number, has been plotted in Figure 17. The importance of each drag contribution, expressed as a percentage of the total drag, is shown in Table XX.

Table XX

Contribution of the Various Drag Components
Expressed as a Percentage of the Total Drag

Mach Number	1.86	2.50	3.24	4.50
C_{D_W} body	11.0	14.9	19.1	33.1
$C_{D_{S.F.}}$ body	15.8	7.0	10.8	23.4
C_{D_B} (body + fins)	61.5	63.7	52.2	13.8
C_{D_W} fins	7.8	8.5	8.8	9.7
$C_{D_{S.F.}}$ fins	3.9	5.9	9.1	20.0
C_D TOTAL	100	100	100	100

64. It is interesting to note the very large increase in drag due to the presence of the fins, as compared with the drag of the bare body, the two drag curves being plotted in Figure 18. Such an increase varies roughly between 50 and 70 percent over the Mach number range considered. Comparison of Tables X, XIX, and XX leads to the following conclusions: The wave drag coefficient of the body alone remains approximately constant in absolute value as the Mach number is varied, but as the total drag coefficient decreases with increasing Mach number, the relative importance of the body wave drag coefficient increases. The variation of the body skin friction coefficient, which, of course, is not changed by the presence of fins, has already been discussed. With regard to the wave drag and the skin friction of the fins themselves, the combination of the two is roughly of the same order of magnitude as the drag of the body due to the head shockwave. Just as in the case of the bare body, the drag due to the base pressure appears to be a very important factor, contributing in the lower Mach number range more than half of the total drag. It is interesting to note that, at a Mach number of 2.5, the contribution of the fins to the sum of the wave drag and skin friction drag coefficients is only 0.049, while the same fins add 0.095 to the base pressure drag coefficient. It should be noted again that what appears to be the largest contribution to the total drag coefficient comes from a component of the drag for which no rigorous analysis seems possible, and for which there still exists a great penury of

reliable and diversified experimental data. Until such a time when these unfortunate circumstances are fully remedied, an "engineering guess" of the total drag coefficient and the drag breakdown is the best that can be hoped for.

CONCLUSIONS

65. It is hoped that the method presented may be used to obtain reliable estimates of the drag coefficients of four-finned missiles in the wind tunnels, in the ranges, and in free-flight at full scale. The practical value of this method may be determined only after the results of a number of computations for different conditions are compared with the corresponding experimental data. Like any empirical method strongly based on experimental information, this method should be improved as more refined experimental data are available. The correlations made so far are very satisfactory. They have not been presented here because they are not yet sufficiently numerous or independent, and might cause the reader to attribute to the method a greater reliability than it actually deserves.

Acknowledgement

66. The author wishes to express his gratitude to Mr. Charles J. Kulishek who, beside giving general assistance in the preparation of this Report, contributed extensively to the paragraphs dealing with the fin wave drag component.

List of Symbols

Δp = $p_s - p_1$

p_s = pressure at the surface of the body

p_1 = static pressure of the undisturbed stream

q = dynamic pressure, equal to $\frac{\gamma p}{2} M^2$

γ = ratio of specific heats of air

M = Mach number of the undisturbed stream

C_{D_W} = wave drag coefficient

λ = ogive "slenderness" ratio = $\frac{\text{axial length of the ogive}}{\text{radius of the tangent cylinder}}$

L = axial length of the body

D = diameter of the body

K = similarity parameter = $\frac{\text{free-stream Mach number}}{\text{fineness ratio of ogive}}$

ϕ = angle between an elemental area, dA, on the ogival nose and the direction of motion

R = radius of the tangent cylinder, maximum radius of the ogive

N_c = caliber number of the ogive

A = surface area of the ogival nose

u = component of the velocity parallel to the surface of the missile, at a given distance from the nose

y = distance along a direction normal to the surface of the missile, at a given distance from the nose

l = mixing length in turbulent boundary layer

$C_{D_{S.F.}}$ = skin friction drag coefficient, referred to the cylinder cross-sectional area

p_b = pressure at the base of the model

List of Symbols (continued)

C_{D_B} = base pressure drag coefficient

r_u = probable error on the wave drag coefficient

r_v = probable error on the skin friction coefficient

r_w = probable error on the base pressure drag coefficient

R = probable error on the total body drag coefficient

$C_{D_{a_1}}$ = induced drag coefficient of fin

C_L = lift coefficient of fin

C_{D_b} = wave drag coefficient of fin resulting from the thickness distribution

C_{D_c} = wave drag coefficient of fin resulting from the camber distribution

μ = local slope of the wing surface

β = $\sqrt{M^2-1}$

m = ratio of the slope of the fin leading edge to the Mach line slope

m_t = ratio of the slope of the fin trailing edge to the Mach line slope

a_t = ratio of the slope of a ray connecting the fin leading edge vertex and the tip trailing edge to the Mach line slope

A_{BE} = area of the beveled edge projected on the chord line

a, h = length of sides of the beveled edge projection on the chord line

ψ = included angle of the beveled edge

p3 = static pressure before the shock produced by the fin

p_{o3} = stagnation pressure before the shock produced by the fin

p_{o1} = stagnation pressure before the shock produced by the missile nose

p2 = static pressure behind the shock produced by the fin section through the horizontal plane

List of Symbols (continued)

p_{bf} = static pressure at the base of the fin

s = fin semi-span; vertical length of the fin leading-edge

t = fin semi-thickness

α = shock angle

A_c = body cross-sectional area

ϕ = angle between the elemental surface and the direction of motion

θ = angle made by the tangent to the ogival contour at a point (x, y) with the ogival axis

Re = Reynolds number

b_1 = horizontal length of the fin leading edge

b_2 = length of fin tip chord

h = chordwise distance from the fin leading edge to the point of maximum thickness

C_f = skin friction factor, referred to the unit area of wetted skin

References

(a) Halbmillion, V., McGraw, H. A Method of Determining, Approximately, the Pressure Distribution on the Ogival Noses of Missiles, Based on an Extension of Taylor-Maccoll Calculations. NOLM 9816 (1949)
(b) Miles, E. R. C. Semi-Empirical Formulas for Ogives. APL/JHU CM-505 (1948)
(c) Taylor, G. I., Maccoll, J. W. The Air Pressure on a Cone Moving at High Speeds. Proc. Roy. Soc. (A), 139, 278-311, London (1933)
(d) Fowler, J. E., French, D. M. A Graphical Correlation Based on the Taylor-Maccoll Results of the Air Conditions Just Outside the Boundary Layer of a Cone as Related to the Conditions of the Undisturbed Air. Data Folder 85501 GE Co., Schenectady, N.Y. (1946)
(e) Tsien, H. S. Similarity Laws of Hypersonic Flows. Jour. Math. and Physics, Vol 25, No. 3 (1946)
(f) Ehret, D. M., Rossow, V. J., Stevens, V.I. An Analysis of the Applicability of the Hypersonic Similarity Law to the Study of Flow About Bodies of Revolution at Zero Angle of Attack. NACA TN 2250 (1950)
(g) Rossow, V. J. Applicability of the Hypersonic Similarity Rule to Pressure Distributions Which Include the Effects of Rotation for Bodies of Revolution at Zero Angle of Attack. NACA TN 2399 (1951)
(h) Rubesin, M. W., Maydew, R. C., Varga, S. A. An Analytical and Experimental Investigation of the Skin Friction of the Turbulent Boundary Layer. NACA TN 2304 (1951)
(i) Wilson, R. E. Turbulent Boundary Layer Characteristics at Supersonic Speeds. U. of Texas DRL CM-569 (1949)
(j) Thomas, R. N. Some Comments on the Effect of Adding Length to the Afterbody of a Square-based, Conical-headed Projectile. BRL Rpt. No. 543 (1945)
(k) Kurzweg, H. H. The Pressure at the Base of Bodies at Supersonic Speeds. NOLM 9609 (1948)
(l) Kurzweg, H. H. New Experimental Investigations on Base Pressure in the NOL Supersonic Wind Tunnels at Mach Numbers 1.2 to 4.24. NOLM 10113 (1950)
(m) Charters, A.C. Some Ballistic Contributions to Aerodynamics. Jour. of Aero. Sci., Mar 1947, pp 155 to 167
(n) Kuethe, A. M., Epstein, H. T. Viscosity Effects in Transonic and Supersonic Flow. Bumblebee Series Rpt. No. 48, Dept. of Engr. Res. of the U. of Mich. (1946)
(o) Lapin, E. Charts for the Computation of Lift and Drag of Finite Wings at Supersonic Speeds. Rpt. SM-13480, Douglas Aircraft Co. (1949)
(p) Moeckel, W. E., Connors, J. F. Charts for the Determination of Supersonic Air Flow Against Inclined Planes and Axially Symmetric Cones. NACA TN 1373, Flight Propulsion Res. Lab. (1947)
(q) Handbook of Supersonic Aerodynamics. NavOrd Rpt. 1488, Vol 2 (1950)

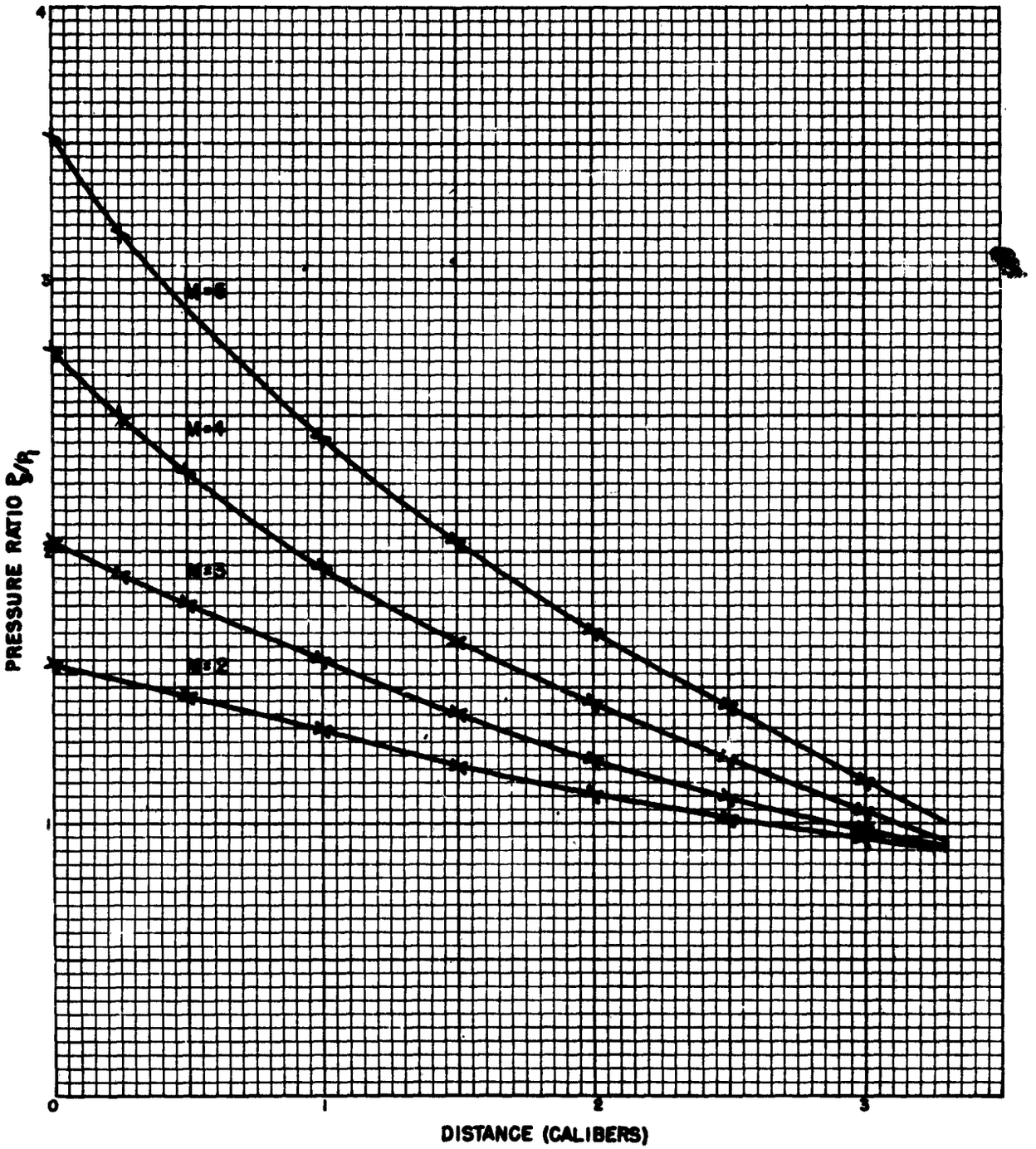

FIG. 1 PRESSURE DISTRIBUTION ON A 14-CALIBER OGIVE

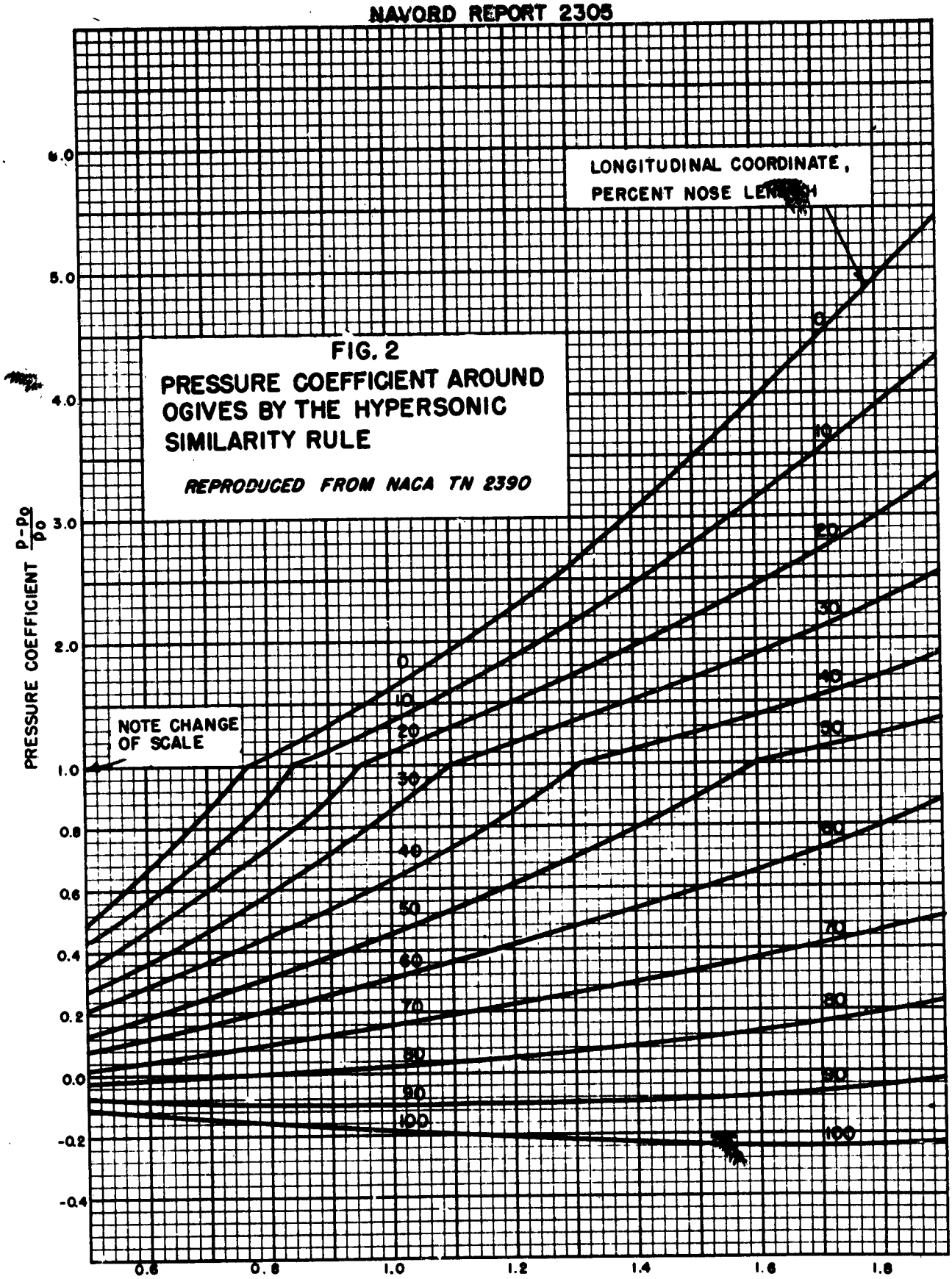

FIG. 2
PRESSURE COEFFICIENT AROUND OGIVES BY THE HYPERSONIC SIMILARITY RULE

REPRODUCED FROM NACA TN 2390

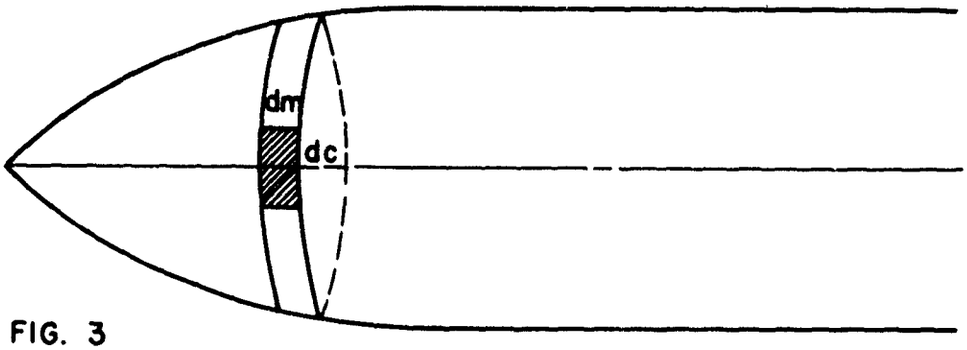

FIG. 3

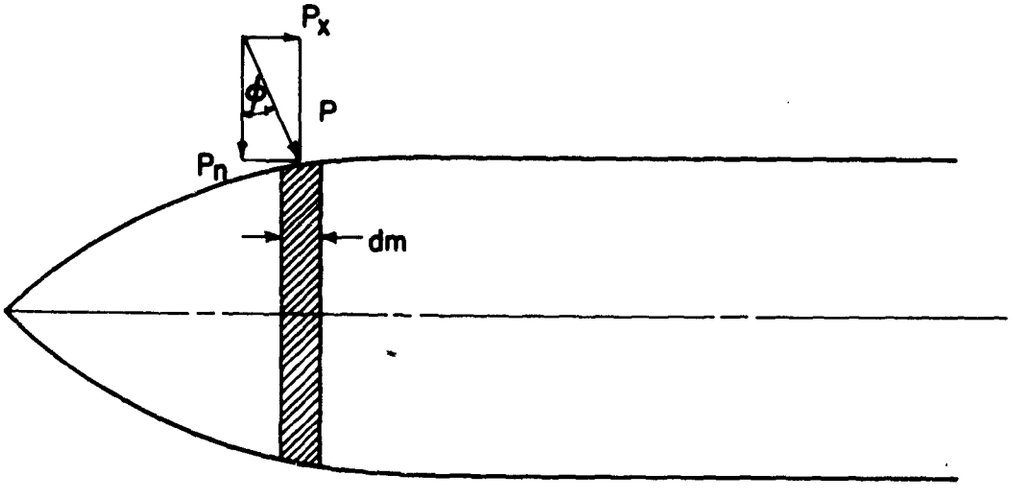

FIG. 4

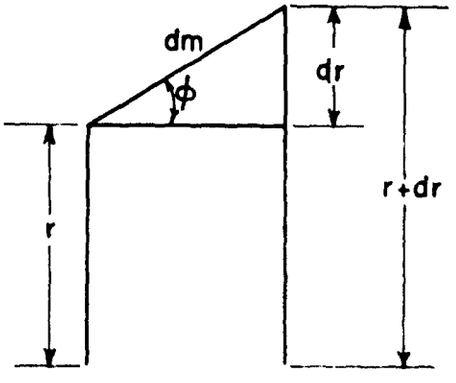

FIG. 5

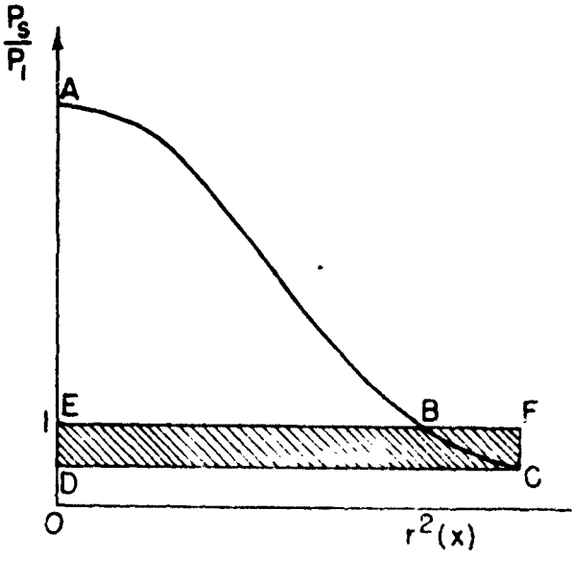

FIG. 6

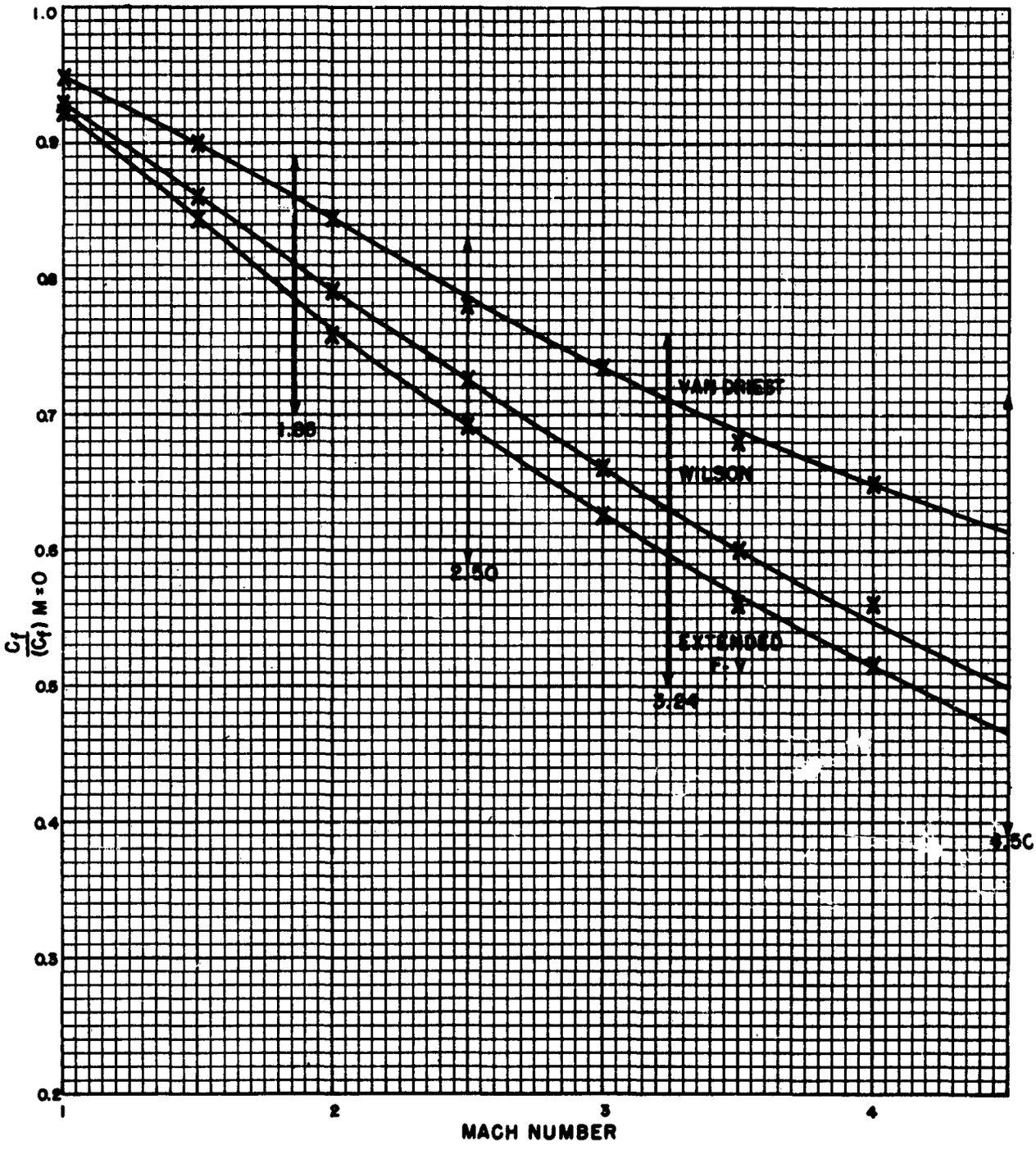

FIG. 7 COMPARISON OF VARIOUS ANALYSES OF THE TURBULENT BOUNDARY LAYER
NOL WIND-TUNNEL CONDITIONS

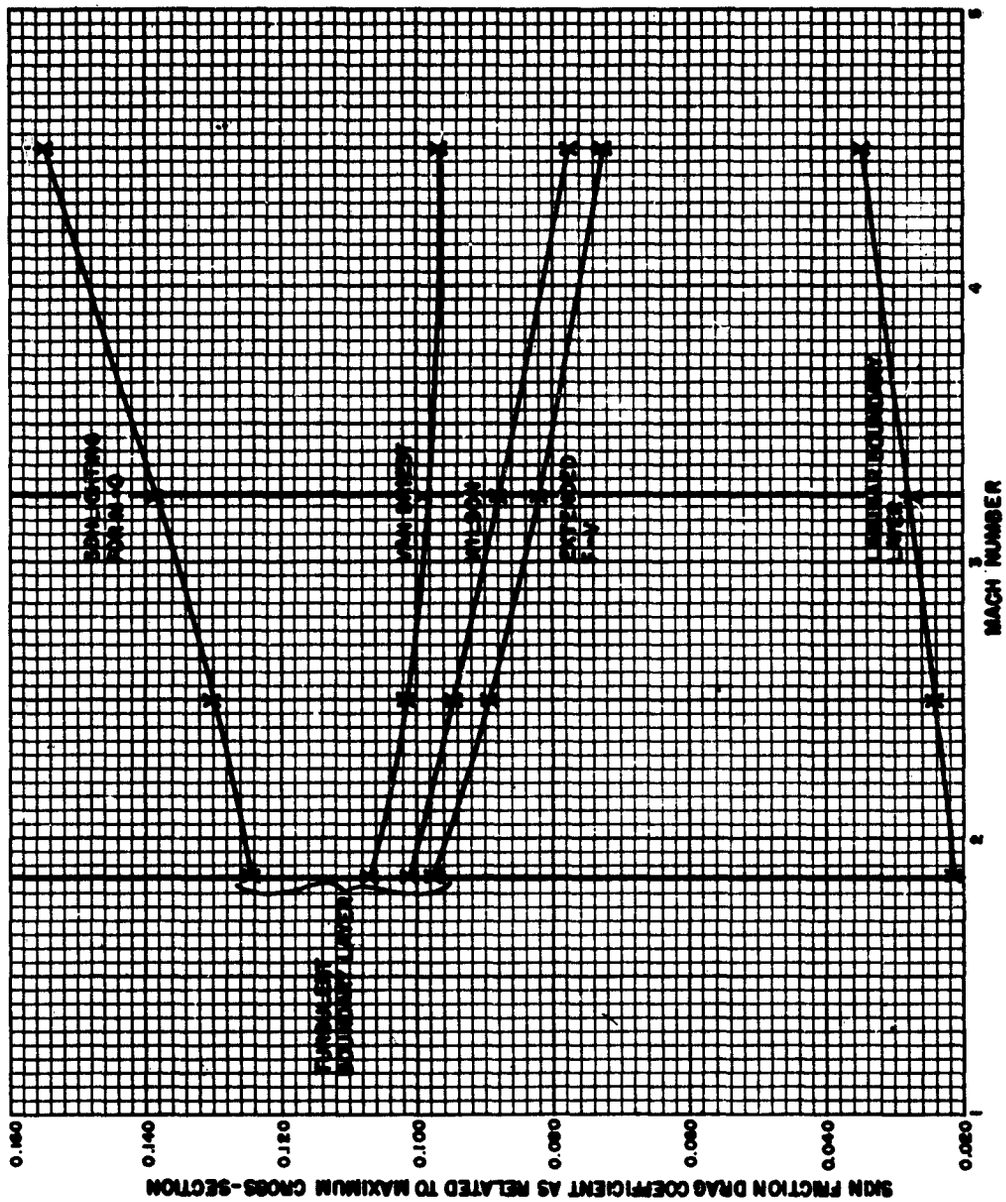

FIG. 8 SKIN FRICTION DRAG COEFFICIENTS FOR AAP AS DETERMINED BY SEVERAL METHODS
NOL WIND-TUNNEL CONDITIONS

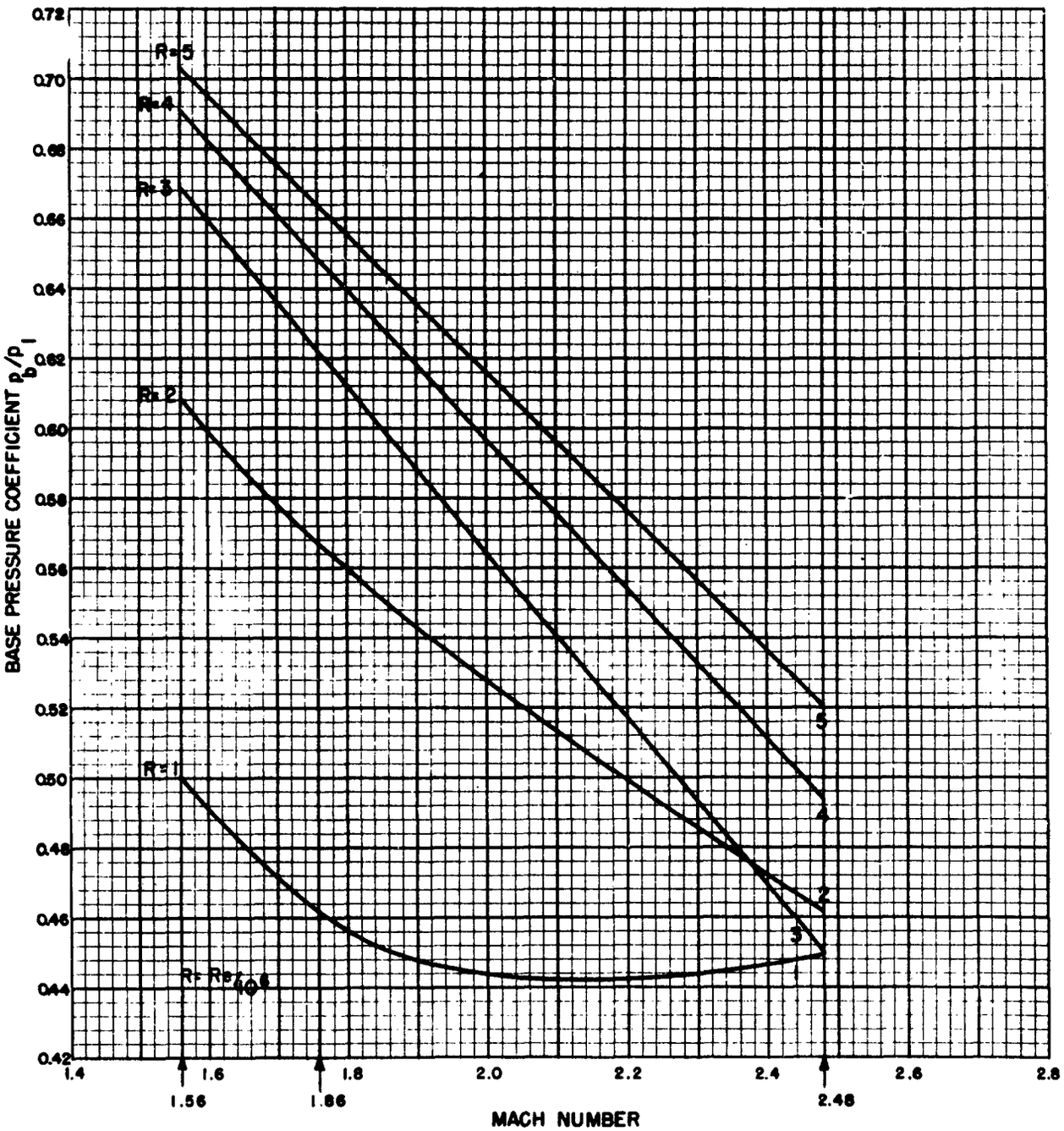

FIG. 9 BASE PRESSURE COEFFICIENT VS MACH NUMBER WITH REYNOLDS NUMBER, Re, AS PARAMETER

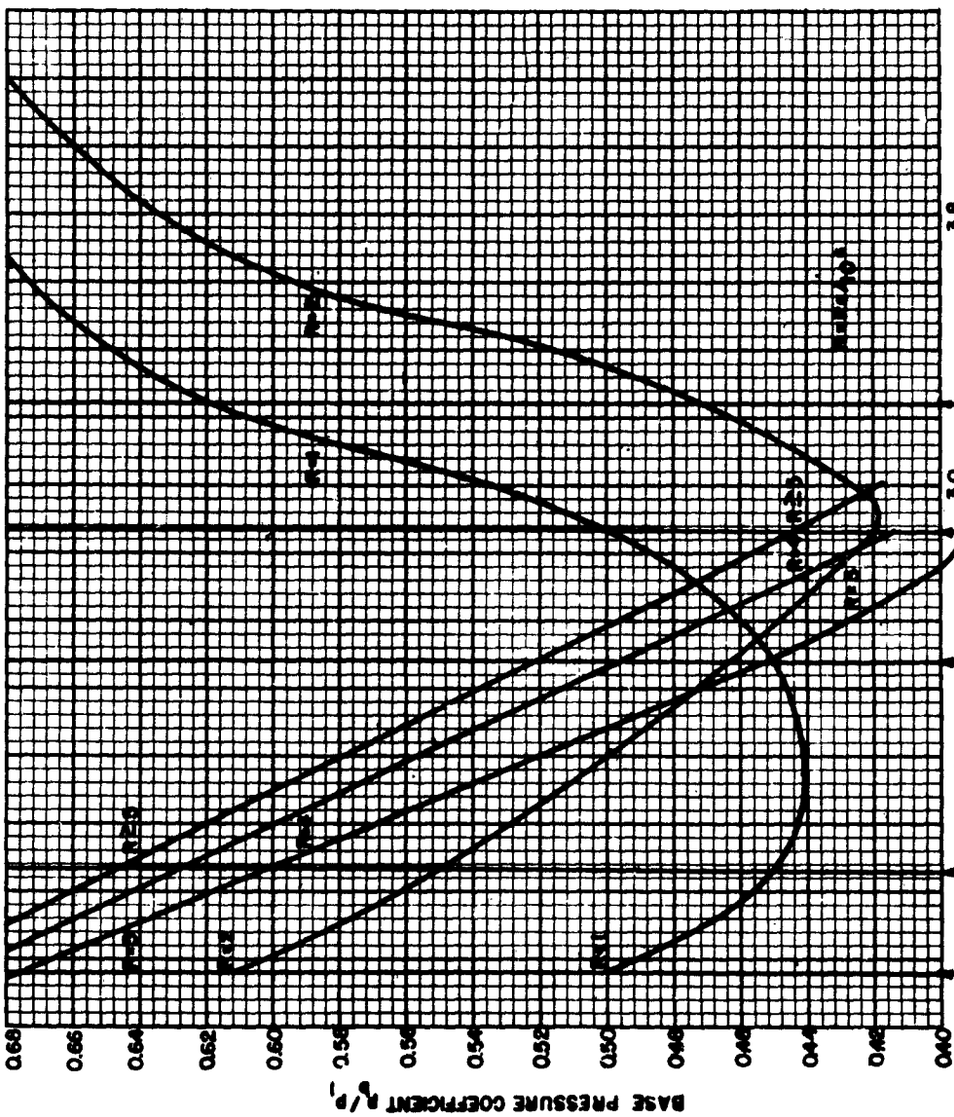

FIG. 10 BASE PRESSURE COEFFICIENT VS MACH NUMBER WITH REYNOLDS NUMBER, Re, AS PARAMETER

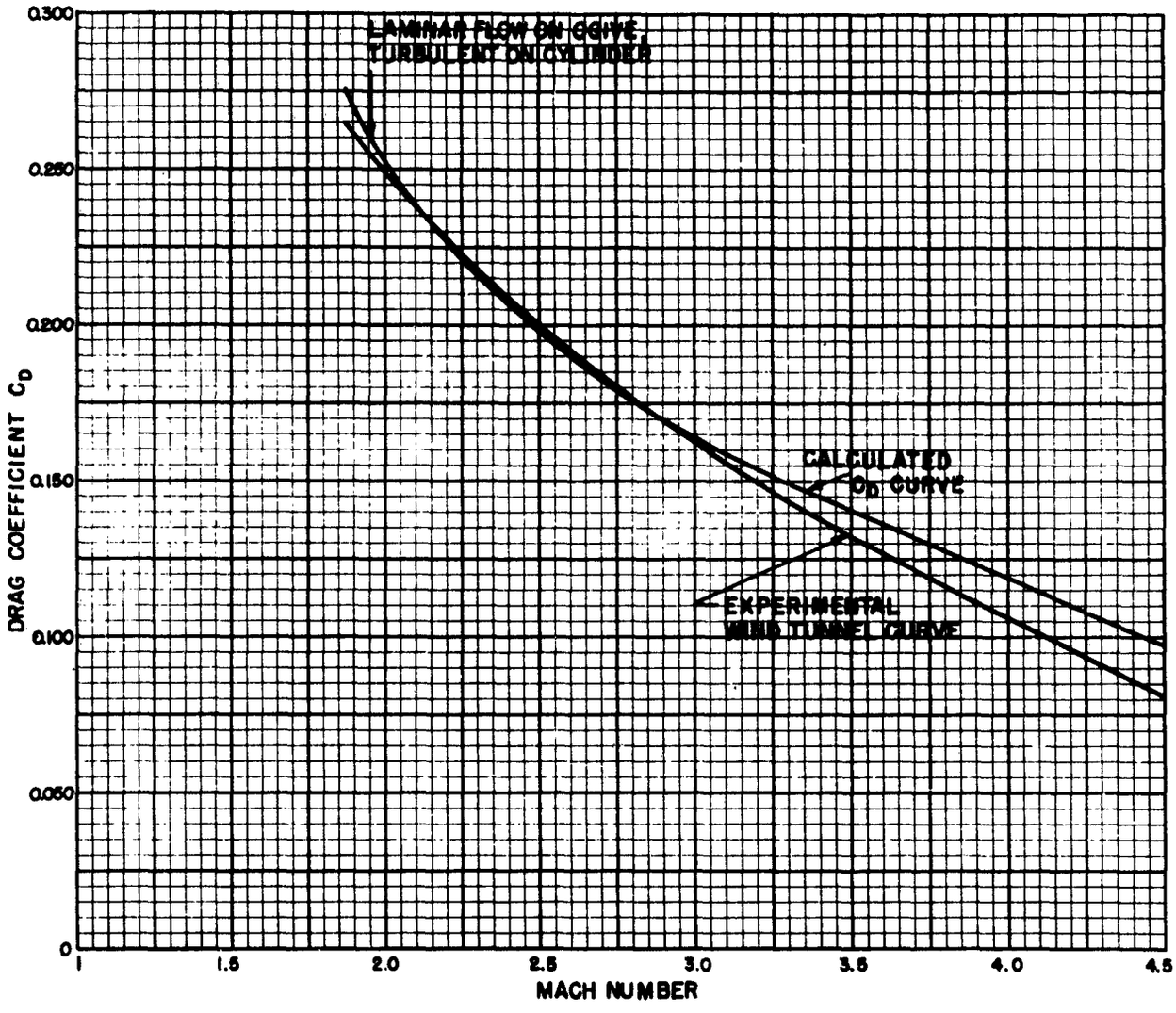

FIG. 11 ESTIMATED DRAG OF AAP (BODY ALONE), COMPARISON WITH EXPERIMENTAL RESULTS

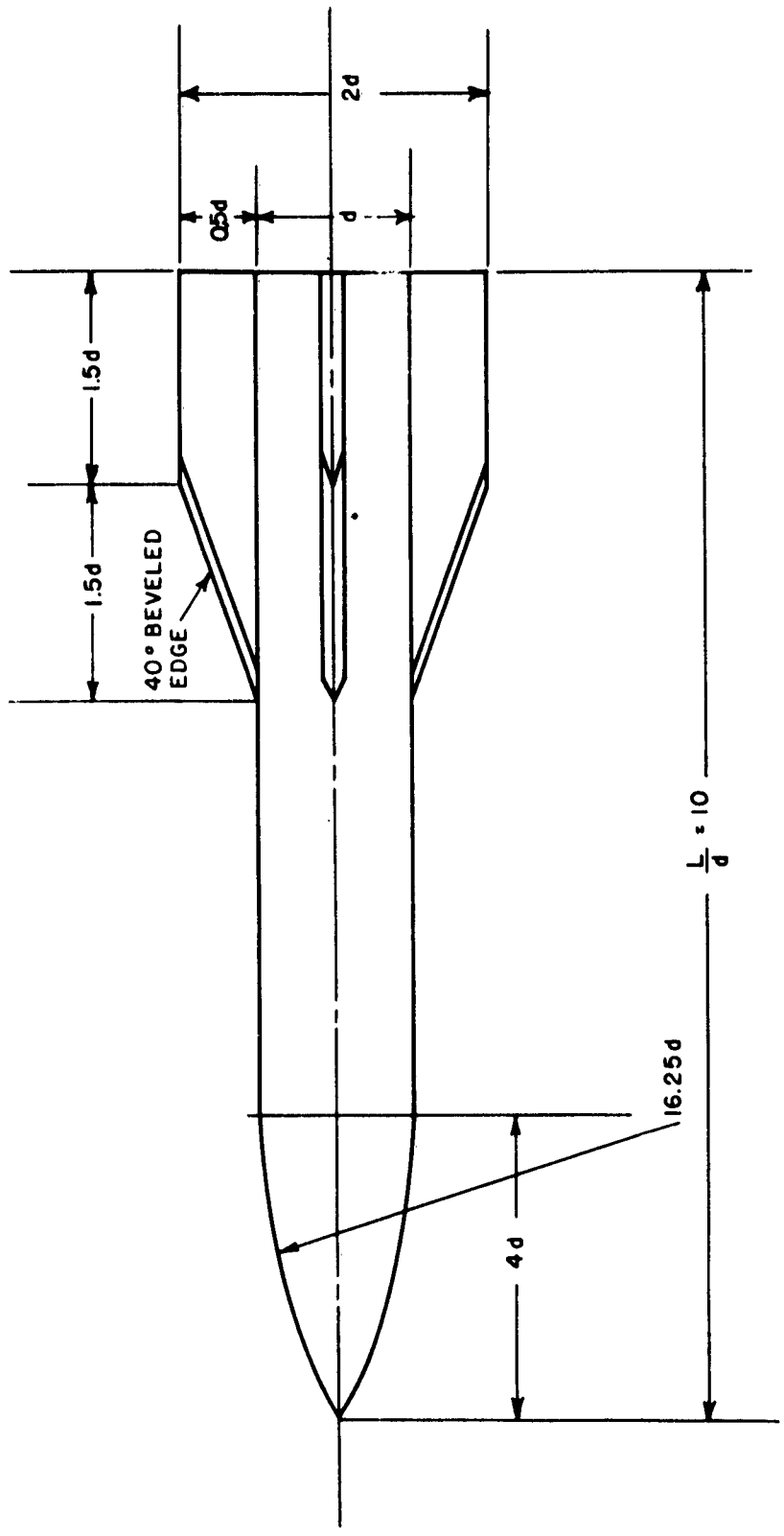

NOTE: ALL DIMENSIONS IN CALIBERS
DRAWING NOT TO SCALE

FIG. 12 ORIGINAL CONFIGURATION, ANGLED ARROW PROJECTILE

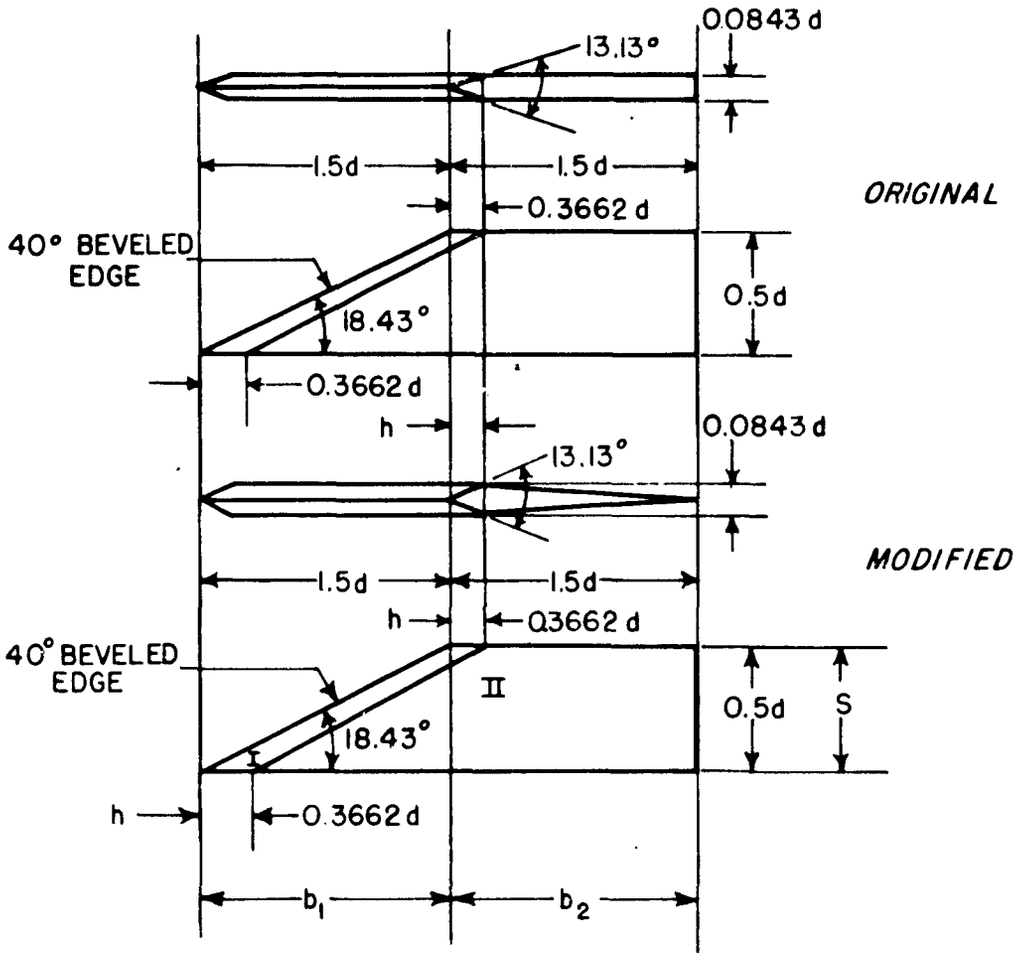

NOTE: ALL DIMENSIONS IN CALIBERS

FIG. 13 MODIFIED FIN CONFIGURATION OF THE AAP

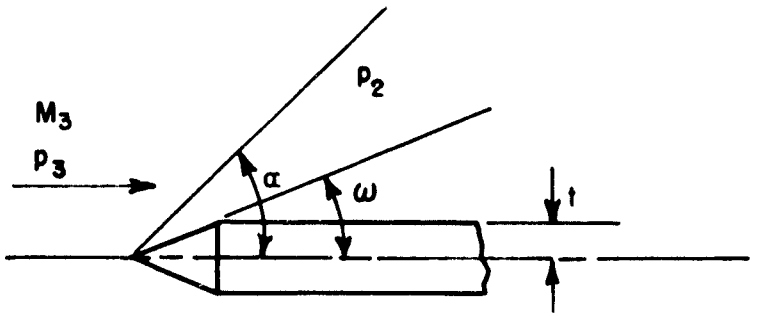

FIG. 14 FIN SECTION THROUGH HORIZONTAL PLANE

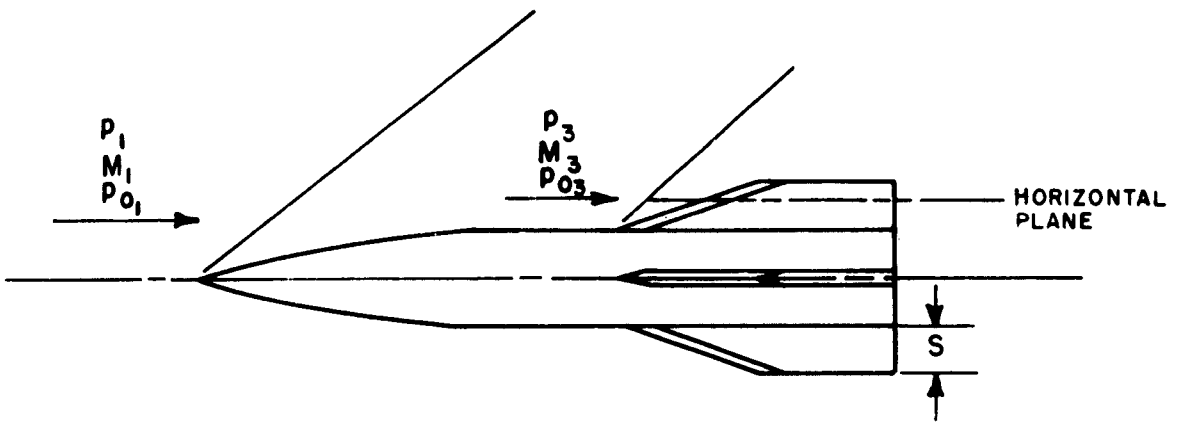

NOTE: DRAWINGS NOT DRAWN TO SCALE

FIG. 15 FIN PLANFORM OF AAP

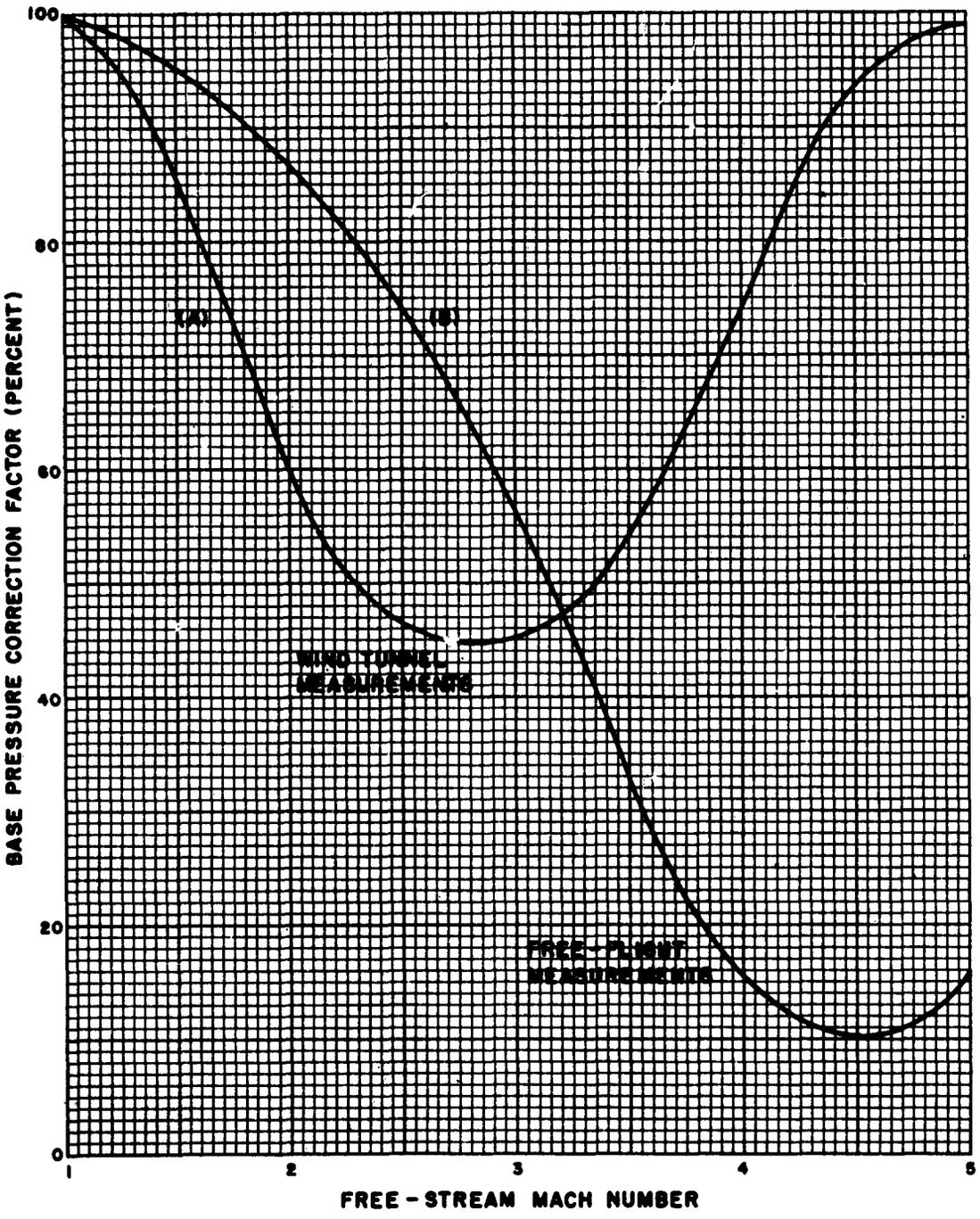

FIG. 16 BASE PRESSURE CORRECTION DUE TO INFLUENCE OF FOUR FINS

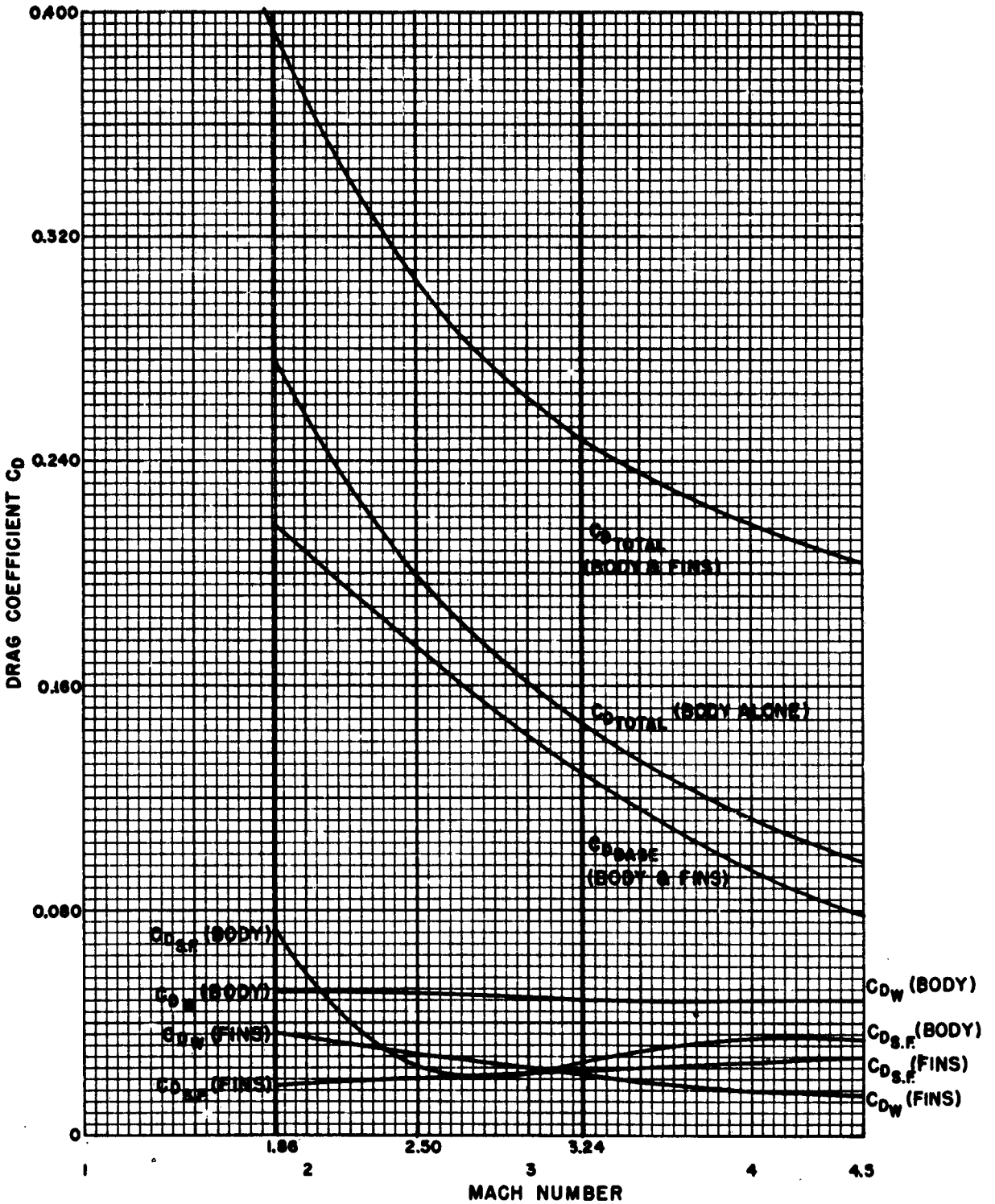

FIG. 17 DRAG BREAKDOWN OF FINNED MISSILE AT VARIOUS WIND-TUNNEL MACH NUMBERS

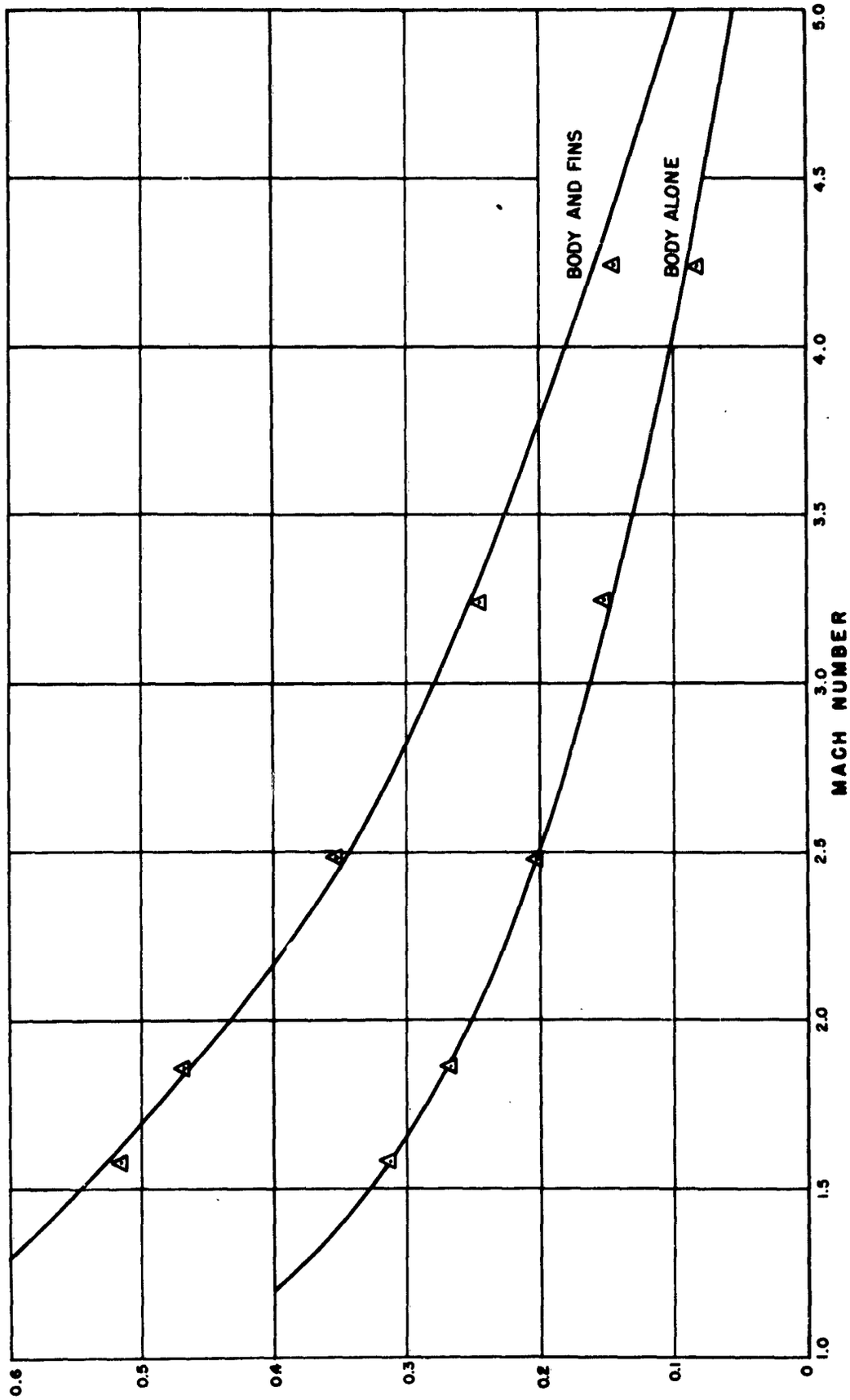

FIG. 18 COMPARISON BETWEEN EXPERIMENTAL RESULTS OF TOTAL DRAG FOR THE BODY ALONE AND FOUR-FINNED MISSILE

Aeroballistic Research Department
External Distribution List for Aeroballistics Research (XI)

No. of Copies	
	Chief, Bureau of Ordnance Department of the Navy Washington 25, D.C.
1	Attn: Rea
1	Attn: Rexe
1	Attn: Re3d
2	Attn: Re6
3	Attn: Re9a
	Chief, Bureau of Aeronautics Department of the Navy Washington 25, D. C.
1	Attn: AER-TD-414
2	Attn: RS-7
	Commander U. S. Naval Ordnance Test Station Inyokern P.O. China Lake, California
2	Attn: Technical Library
1	Attn: Code 5003
	Commander U.S. Naval Air Missile Test Center Point Mugu, California
2	Attn: Technical Library
	Superintendent U.S. Naval Postgraduate School Monterey, California
1	Attn: Librarian
	Commanding Officer and Director David Taylor Model Basin Washington 7, D. C.
2	Attn: Hydrodynamics Laboratory
	Chief of Naval Research Library of Congress Washington 25, D. C.
2	Attn: Technical Info. Div.
	Office of Naval Research Department of the Navy Washington 25, D. C.
1	Attn: Code 438
2	Attn: Code 463
	Director Naval Research Laboratory Washington 25, D. C.
1	Attn: Code 2021
1	Attn: Code 3800
1	Officer-in-Charge Naval Aircraft Torpedo Unit U.S. Naval Air Station Quonset Point, Rhode Island
	Office, Chief of Ordnance Washington 25, D. C.
1	Attn: ORDTU

No. of Copies	
2	Library Branch Research and Development Board Pentagon 3D1041 Washington 25, D.C.
	Chief, AFSWP P.O. Box 2610 Washington 25, D. C.
1	Attn: Technical Library
1	Chief, Physical Vulnerability Branch Air Targets Division Directorate of Intelligence Headquarters, USAF Washington 25, D. C.
	Commanding General Wright Air Development Center Wright-Patterson Air Force Base Dayton, Ohio
5	Attn: WCAPD
1	Attn: WCSD
2	Attn: WCSOR
2	Attn: WCRRN
1	Attn: WCACD
1	Attn: WCRRF
1	Director Air University Library Maxwell Air Force Base, Alabama
	Commanding General Aberdeen Proving Ground Aberdeen, Maryland
1	Attn: C.L. Poor
1	Attn: D.S. Dederick
	National Bureau of Standards Washington 25, D.C.
1	Attn: Nat'l Applied Math. Lab.
1	Attn: Librarian (Ord. Dev. Div.)
1	Attn: Chief, Mechanics Div.
	National Bureau of Standards Corona Laboratories (Ord. Dev. Div.) Corona, California
1	Attn: Dr. H. Thomas
	National Bureau of Standards Building 3U, UCLA Campus 405 Hilgard Avenue Los Angeles 24, California
1	Attn: Librarian
	University of California 211 Mechanics Building Berkeley 4, California
1	Attn: Dr. R. G. Folsom
1	Attn: Mr. G. J. Maslach
1	Attn: Dr. S. A. Schaaf VIA: InsMat

No. of Copies	
	California Institute of Technology Pasadena 4, California
2	Attn: Librarian(Guggenheim Aero Lab)
1	Attn: Dr. H.T. Nagamatsu
1	Attn: Prof. M.S. Plesset
1	Attn: Prof. F. Goddard
1	Attn: Dr. Hans W. Liepman
	VIA: BuAero Representative
	College of Engineering Cornell University Ithaca, New York
1	Attn: Prof. A. Kantrowitz
	VIA: ONR
	University of Illinois 202 E. E. R. L. Urbana, Illinois
1	Attn: Prof A. H. Taub
	VIA: InsMat
1	Director Inst. for Fluid Dynamics and Applied Math University of Maryland College Park, Maryland
	VIA: InsMat
	Massachusetts Inst. of Technology Cambridge 39, Massachusetts
1	Attn: Prof. G. Stever
1	Attn: Prof. J. Kaye
	VIA: InsMat
	University of Michigan Ann Arbor, Michigan
1	Attn: Prof. Otto Laporte
	VIA: InsMat
	University of Michigan Willow Run Research Center Ypsilanti, Michigan
1	Attn: L.R. Biasell
	VIA: InsMat
	University of Minnesota Rosemount, Minnesota
1	Attn: J. Leonard Frame
1	Attn: Prof. N. Hall
	VIA: Ass't InsMat
	The Ohio State University Columbus, Ohio
2	Attn: G. L. Von Eschen
	VIA: Ass't InsMat
	Polytechnic Institute of Brooklyn 99 Livingston Street Brooklyn 2, New York
1	Attn: Dr. Antonio Ferri
	VIA: ONR
	Princeton University Princeton, New Jersey
1	Attn: Prof. S. Bogdonoff
1	Attn: Prof. L. Lees
	VIA: ONR

No. of Copies	
	Massachusetts Inst. of Technology Cambridge 39, Massachusetts
2	Attn: Project Meteor
1	Attn: Guided Missiles Library
1	Princeton University Forrestal Research Center Library Project Squid Princeton, New Jersey
	Armour Research Foundation 35 West 33rd Street Chicago 16, Illinois
1	Attn: Engr. Mech. Div.
	VIA: ONR
	Applied Physics Laboratory The Johns Hopkins University 8621 Georgia Avenue Silver Spring, Maryland
1	Attn: Arthur G. Norris
	VIA: NIO
1	Cornell Aeronautical Lab., Inc. 4455 Genesee Street Buffalo 21, New York
	VIA: BuAero Rep.
1	Defense Research Laboratory University of Texas Box 1, University Station Austin, Texas
	VIA: InsMat
	Eastman Kodak Company 50 W. Main Street Rochester 4, New York
1	Attn: Dr. Herbert Trotter, Jr.
	VIA: NIO
	General Electric Company Building #1, Campbell Avenue Plant Schenectady, New York
1	Attn: Joseph C. Hoffman
	VIA: InsMachinery
	The Rand Corporation 1500 Fourth Street Santa Monica, California
1	Attn: The Librarian
	VIA: InsMat
	Consolidated Vultee Aircraft Corp. Daingerfield, Texas
1	Attn: J.E. Arnold
	VIA: Dev. Contract Office
	Douglas Aircraft Company, Inc. 3000 Ocean Park Boulevard Santa Monica, California
1	Attn: Mr. E.F. Burton
	VIA: BuAero Resident Rep.

No. of Copies

North American Aviation, Inc.
12214 Lakewood Boulevard
Downey, California
2 Attn: Aerophysics Library
VIA: BuAero Representative

United Aircraft Corporation
East Hartford 8, Connecticut
1 Attn: Robert C. Sale
VIA: BuAero Representative

National Advisory Committee for Aero
1724 F Street, Northwest
Washington 25, D. C.
5 Attn: E. B. Jackson

Ames Aeronautical Laboratory
Moffett Field, California
1 Attn: H.J. Allen
2 Attn: Dr. A.C. Charters

NACA Lewis Flight Propulsion Lab.
Cleveland Hopkins Airport
Cleveland 11, Ohio
1 Attn: John C. Evvard

Langley Aeronautical Laboratory
Langley Field, Virginia
1 Attn: Theoretical Aerodynamics Div.
1 Attn: J. V. Becker
1 Attn: Dr. Adolf Buseman
1 Attn: Mr. C. H. McLellan
1 Attn: Mr. J. Stack

Harvard University
21 Vanserg Building
Cambridge 38, Massachusetts
1 Attn: Prof. Garrett Birkhoff

The Johns Hopkins University
Charles and 34th Streets
Baltimore 18, Maryland
1 Attn: Dr. Francis H. Clauser

New York University
45 Fourth Avenue
New York 3, New York
1 Attn: Professor R. Courant

1 Dr. Allen E. Puckett, Head
Missile Aerodynamics Department
Hughes Aircraft Company
Culver City, California

1 Dr. Gordon N. Patterson, Director
Institute of Aerophysics
University of Toronto
Toronto 5, Ontario, Canada
VIA: BuOrd (Ad8)